geologicaacta

Citation: Illueca, N., Liesa, C.L., Soria, A.R., 2024. Linking high-frequency lacustrine sequences to orbitally-induced cyclicity (Lower Cretaceous, Iberian Basin). Geologica Acta, 22.10, 1-26.
Online ISSN: 1696-5728 DOI: 10.1344/GeologicaActa2024.22.10

Linking high-frequency lacustrine sequences to orbitally-induced cyclicity (Lower Cretaceous, Iberian Basin)

Natalia Illueca Carlos L. Liesa Ana R. Soria

Dpto. de Ciencias de la Tierra, Grupo GEOtransfer - Instituto Universitario de Investigación en Ciencias Ambientales de Aragón (IUCA), Universidad de Zaragoza
Pedro Cerbuna 12, 50009 Zaragoza, Spain
Illueca E-mail: nillueca@unizar.es, Illueca ORCID: 0009-0008-9396-5915
Liesa E-mail: carluis@unizar.es, Liesa ORCID: 0000-0002-9130-117X
Soria E-mail: anasoria@unizar.es, Soria ORCID: 0000-0003-2963-8422

ABSTRACT

The lacustrine El Castellar Formation in the Castillo de Aliaga section (Early Cretaceous Galve sub-basin, eastern Spain) features two carbonate successions of marl and limestone, separated by a mudstone and marl interval. Sequence analysis revealed small-scale (44 elementary sequences), medium-scale (ten complete and two incomplete parasequences), and large-scale (three sets of parasequences, one incomplete), high-frequency lacustrine sequences, with an average thickness of 2.9, 12.4 and 54m, respectively. These sequences start with a sudden facies change (deepening) and exhibit a shallowing-upward trend with features of subaerial exposure (bioturbation, oxidation, or brecciation) at the top, indicating phases of climate-modulated lake expansion and retraction. The temporal framework of the lacustrine sequences is further characterized by the correlation of these sequences with sedimentary-cycle periodicities of 3.3, 13.2 and 57.3m, attributed, respectively, to the long precession cycle (22.4kyr) and the short (95kyr) and long (405kyr) eccentricity cycles of the Earth's orbit. The hierarchical stacking of sequences aligns with orbitally driven cyclicity, with thickness variations interpreted as tectonic subsidence effects (accommodation) resulting from normal fault slip in a rift system. The three sets of parasequences (SPS-1 to SPS-3) align with stages of lake system evolution. SPS-1 represents deposition in a low-energy shallow carbonate lake. SPS-2 indicates a significant lake expansion and deepening, linked with clastic input and a mixed lake system, and correlates with a major increase in accommodation, over ~200kyr, involving fault-induced local tilting. SPS-3 represents deposition in a high-energy carbonate lake. The parasequences identified show variations in cyclic thickness tied to a >700kyr tectonic cycle. The elementary sequences, mainly corresponding to marl-limestone bundles, exhibit thickness changes probably due to shorter-term tectonic pulses. Accelerated tectonic activity resulted in increased accommodation in shorter (40-50kyr) periods, followed by longer (>100kyr) periods of progressive deceleration.

KEYWORDS **Lacustrine facies. Sequence stratigraphy. Climatic forcing. Milankovitch cycles. Tectonic forcing.**

INTRODUCTION

Lacustrine systems are depositional settings that are quite sensitive to environmental changes, forced primarily by variations in climate but also in tectonics (*e.g.* Argylian and Forman, 2003; Armenteros and Huerta, 2006; Gierlowski Kordesch *et al.*, 1991; Jin *et al.*, 2020; Meléndez *et al.*, 2009; Moreno *et al.*, 2012; Sáez *et al.*, 2009; Scheidt *et al.*, 2020; Wei *et al.*, 2018). These factors mainly affect the level and depth of the lake's water, the terrestrial input, the productivity of carbonates, and the flow of groundwater, thus modulating the environmental evolution of the lake and consequently the sedimentary pattern recorded in the lake basin (Carroll and Bohacs, 1999; de Wet *et al.*, 2015; Gómez-Fernández and Meléndez, 1994; Kovács *et al.*, 2021; Ming *et al.*, 2020; Rits *et al.*, 2017; Woolway *et al.*, 2020). Nevertheless, disentangling the signal and response of each of these factors, or their interaction and relative contribution, in relation to the environmental changes recorded in the sedimentation, is not an easy task.

In this regard, cyclostratigraphy is a helpful tool. By conducting spectral analysis of various paleoclimatic proxies in the lake record (*e.g.* lithology, carbonate content, magnetic susceptibility, the gamma-ray signal, color parameters of the sediments, and distality-ranked lacustrine facies), orbitally induced climate cycles (Milankovitch cycles; Milankovitch, 1941) related to changes in the Earth's insolation can be detected. Interpreting the recorded cyclicity can thus provide valuable insights into past climate variations and trends (*e.g.* Aziz *et al.*, 2000; Ezquerro *et al.*, 2022a; Juhász *et al.*, 1997; Hoorn *et al.*, 2022; Lepre and Quinn, 2022; Schnyder *et al.*, 2009; Valero *et al.*, 2014; Zhong *et al.*, 2022).

The astronomical forcing of lake sedimentary records has been assessed in both recent (Anselmetti *et al.*, 2006; Camuera *et al.*, 2018; Coianiz *et al.*, 2019; Guiter *et al.*, 2003; Kuzucuoğlu *et al.*, 1997; Tian *et al.*, 2017; Wei *et al.*, 2020; Zhong *et al.*, 2015) and ancient lakes (Gomes *et al.*, 2020; Huang *et al.*, 2020; Ielpi, 2012; Li *et al.*, 2018; Tang *et al.*, 2023; Wei *et al.*, 2023; Xu *et al.*, 2023). Climatic cyclicity is often well recorded even in lakes with active tectonics capable of modifying the accommodation and, therefore, the rate of sediment accumulation (Azennoud *et al.*, 2023; Deino *et al.*, 2006; Luzón *et al.*, 2002; Morrill *et al.*, 2001; Soria *et al.*, 2012; Steenbrink *et al.*, 2006; Walzer and Hendel, 2023; Wang *et al.*, 2012). This is common, for example, in the Cretaceous lacustrine synrift basins of Iberia (Angulo and Muñoz, 2013; Casas *et al.*, 2024; Liesa *et al.*, 2023; Muñoz *et al.*, 2020; Navarrete, 2015; Soria *et al.*, 2012).

Sequence stratigraphy, originally developed to interpret changes in relative sea level in marine successions (Boulila *et al.*, 2011; Catuneanu, 2022; Emery and Meyers, 2009; Posamentier and Vail, 1988), has also been applied with good results to the study of lake successions. Lake sequences are commonly associated with variations in lake levels driven by climatic and environmental changes, providing evidence of external forcing (Azennoud *et al.*, 2023; Changsong *et al.*, 2001; Keighley *et al.*, 2003; Nutz *et al.*, 2017; Oviatt *et al.*, 1994; Wei *et al.*, 2017; Zavala *et al.*, 2022).

In this study, we present a sequence stratigraphy analysis of the lacustrine synrift record of the Early Cretaceous El Castellar Formation in the Galve sub-basin (western Maestrazgo Basin, eastern Spain). By characterizing lacustrine facies and facies associations, we not only interpret the sedimentary environment and the overall evolutionary trend of the lake, but also analyze high-frequency lacustrine sequences at different scales, along with the behavior and patterns of these sequences throughout the lacustrine succession. These results are then integrated with the orbitally forced climatic cycles (long and short eccentricity, and long precession) recently described by Illueca *et al.* (2023) for the studied deposits. This allows us to link the high-frequency lacustrine sequences of different orders to climate changes induced by variations in the Earth's orbit (Milankovitch cycles), despite the significant influence of tectonics expected in this synrift unit. Variations in the thickness of the lacustrine sequences and cycles are interpreted as tectonically forced changes in accommodation and are used to analyse the sequence stacking and describe patterns of tectonic activity recorded in the lacustrine succession.

GEOLOGICAL SETTING

The Cretaceous Galve sub-basin is located in the eastern Iberian Chain (eastern Spain) (Fig. 1A). This intraplate chain was formed in the context of the Cenozoic collision between the Eurasian and African plates, resulting from the tectonic inversion of a Mesozoic rifting area known as the Iberian Basin (Capote *et al.*, 2002; Liesa *et al.*, 2018, 2023). The Mesozoic rifting occurred in several stages, driven primarily by the opening and spreading of the Tethys Sea and the central-north Atlantic (Capote *et al.*, 2002; Salas and Casas, 1993; Salas *et al.*, 2001). During the Late Jurassic–Early Cretaceous rifting stage, the Iberian Basin became compartmentalized, leading to the development of smaller basins and sub-basins (Martín-Chivelet *et al.*, 2019). The Galve sub-basin was one of these sub-basins that developed at the western margin of the Maestrazgo Basin (Fig. 1A-B). The sedimentary record of the Maestrazgo Basin and its sub-basins comprises two synrift sequences separated by a regional unconformity (Liesa *et al.*, 2019): synrift

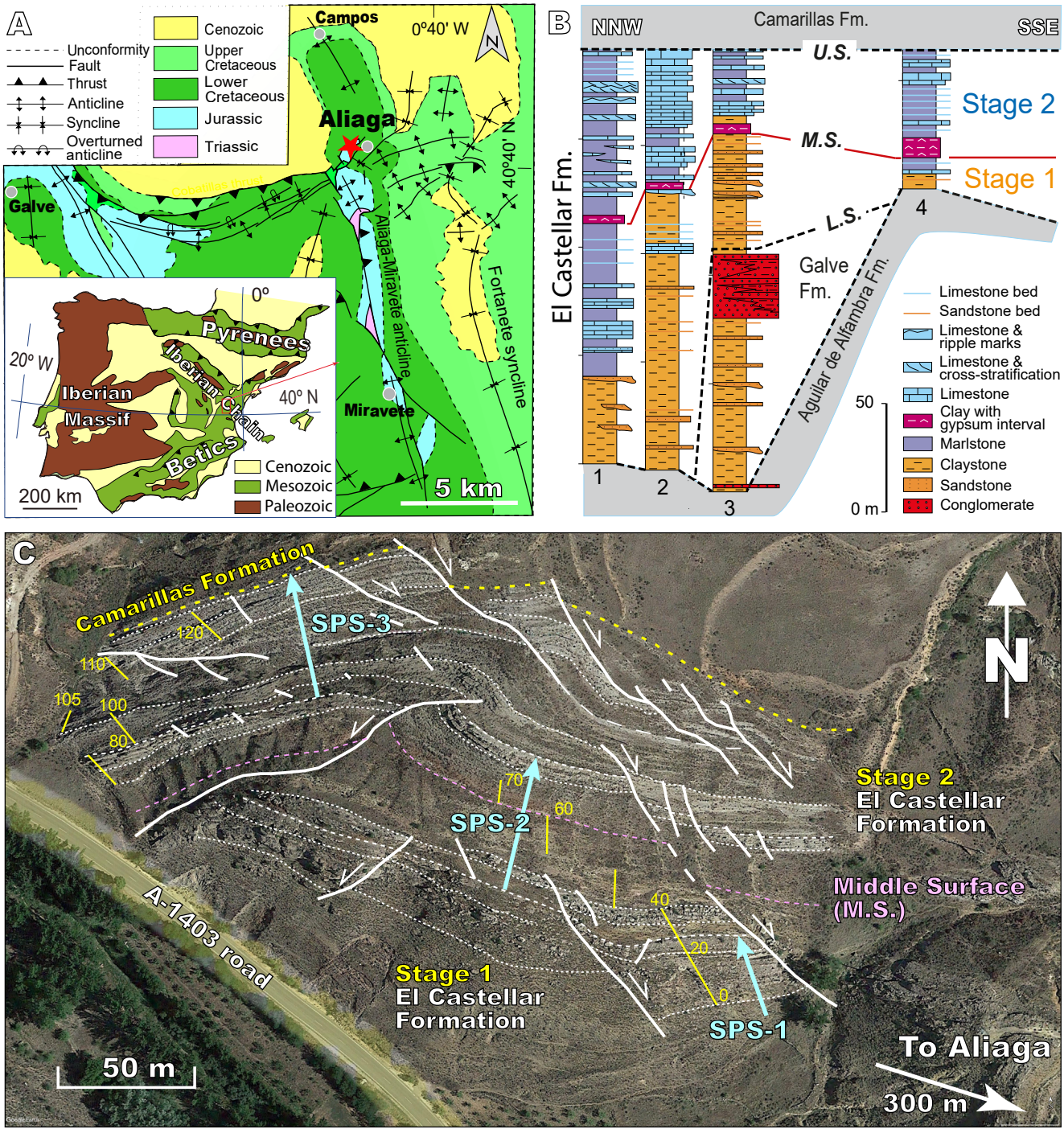

FIGURE 1. A) Geological map of the Aliaga region in western Maestrazgo, showing the location (star) of the Castillo de Aliaga section of the El Castellar Formation (modified from Meléndez *et al.*, 2009). The inset displays the location of the studied section within the Iberian Chain, in eastern Iberian Peninsula (after Liesa *et al.*, 2018). B) Sedimentary succession of the Lower Cretaceous El Castellar Formation in the Galve sub-basin, along with the evolutionary stages of the unit (after Meléndez *et al.*, 2009). Section 1 corresponds to the Castillo de Aliaga section studied here. C) Cartography on aerial imagery displaying the limestone packages (bed lines shown as dashed white lines) of the El Castellar Formation and the normal faults (solid white lines) that displace them. The location of the Castillo de Aliaga section logged in this study is shown with solid yellow lines, with numbers indicating the metres in the stratigraphic series. The Middle Surface (MS; dashed pink line) is used to differentiate the evolutionary stages of this formation. Also depicted are its stratigraphic contact with the overlying Camarillas Formation (dashed yellow line) and the boundaries of the parasequences sets (SPS-1 to SPS-3) distinguished in this study.

sequence 1 (mid Tithonian to Berriasian) and synrift sequence 2 (Valanginian to early Albian).

The El Castellar Formation (Salas, 1987), dating from the late Hauterivian to early Barremian, represents the first unit of synrift sequence 2 in the Galve sub-basin (Aurell *et al.*, 2016; Liesa *et al.*, 2019, 2023). This unit is mainly lacustrine with some alluvial deposits and it lies unconformably over synrift sequence 1 and locally on earlier Jurassic rocks (Fig. 1B) (García-Penas and Aurell, 2017; Liesa *et al.*, 2004, 2006; Meléndez *et al.*, 2009). Its upper boundary is marked by the input of coarse- to medium-grained white sandstones from the fluvial and estuarine Barremian Camarillas Formation (Navarrete, 2015; Soria, 1997; Soria *et al.*, 2023). The thickness of the El Castellar Formation varies significantly (Fig. 1B) due to contemporaneous normal faults trending NNW-SSE and ENE-WSW, which controlled subsidence at different scales, influencing both sedimentation patterns and paleogeography (Liesa *et al.*, 2006, 2019, 2023; Meléndez *et al.*, 2009). This unit consists of a lower alluvial section and an upper lacustrine carbonate section (Fig. 1B), with facies associations belonging to alluvial and palustrine plains, palustrine fringes, a low-energy shallow lake, a mixed siliciclastic-carbonate lake, and a high-energy lake (Aurell *et al.*, 2016; Liesa *et al.*, 2006; Meléndez *et al.*, 2009; Soria, 1997; Soria *et al.*, 2001). In addition to the typical biota of Cretaceous lakes (*e.g.* charophytes, ostracods, and bivalves), this unit also contains dinosaur remains and footprints (*e.g.* Castanera *et al.*, 2022; Gasca *et al.*, 2009; Ruiz Omeñaca, 2006).

The sedimentary evolution of the El Castellar Formation in the Galve sub-basin has been related to the interaction and linkage of normal faults that controlled both the basin structure and the subsidence pattern (Liesa *et al.*, 2006). The alluvial and lacustrine sections correspond to different phases of the rifting process: the alluvial deposits represent the initial rifting stage, whereas the lacustrine deposits mark the onset of the rifting climax (Liesa *et al.*, 2006; Meléndez *et al.*, 2009; Soria *et al.*, 2001). During the initial stage, the basin exhibited a highly heterogeneous distribution of alluvial and palustrine facies, driven by the activity of individual listric faults (Liesa *et al.*, 2006; Soria *et al.*, 2001). In contrast, the subsequent stage is characterized by facies homogenization, marked by the development of a large carbonate lake that covered the entire Galve sub-basin (Meléndez *et al.*, 2009). The transition between these stages is notable for the presence of diagenetic gypsum crystals, which are associated with the fault linkage process. This process likely facilitated the circulation and ascent of highly mineralized water from the Triassic Keuper facies, which contains gypsum (Liesa *et al.*, 2006; Meléndez *et al.*, 2009) (Fig. 1B).

Recently, Illueca *et al.* (2023) conducted a cyclostratigraphic analysis of lithological and magnetic susceptibility data, identifying three main periodicities (~57.3, ~13.2 and ~3.3m). The authors attributed these periodicities respectively to the long eccentricity (405kyr), short eccentricity (95kyr) and long precession (22.4kyr) cycles of the Earth's orbit, suggesting that these orbitally induced cycles correspond to periodic climatic and environmental variations that influenced sedimentation patterns. Despite the area's highly active extensional context, these variations led to the formation of sedimentary sequences that are both recurrent and recognizable.

Regarding the paleoclimatic context, the Cretaceous has traditionally been considered an archetypical supergreenhouse period in the Earth's history (*e.g.* Barron and Washington, 1984; Moriya, 2011; O'Connor *et al.*, 2019; Wang *et al.*, 2014). The Maestrazgo Basin (eastern Iberian Plate) has been located in the subtropical zone (latitude: 26-35ºNorth) during the Barremian (*e.g.* Blakey, 2008; Dercourt *et al.*, 1986; Scotese, 2016; Stampfli and Borel, 2002). Deposition has thus traditionally been assumed to occur under subtropical climatic conditions (Buscalioni and Fregenal-Martínez, 2010; Fölmi, 2012; Haywood *et al.*, 2004; Martín-Chivelet *et al.*, 2019; Ziegler *et al.*, 1987) that fall within the temperate, humid subtropical (Ca) climatic zone in the Hauterivian-Barremian paleo-Köppen climate map (Burgener *et al.*, 2023); that is, the climate was fairly warm, humid and seasonal and conducive to significant paleoweathering (Yuste *et al.*, 2015). However, our growing understanding of the global paleoclimate and sea-level changes (*e.g.* Sames *et al.*, 2016; Hasegawa *et al.*, 2022; Rodríguez-López *et al.*, 2022; Wang *et al.*, 2023, and references therein) has revealed more complex and variable paleoclimatic conditions during the Cretaceous, with an episodically active Early Cretaceous cryosphere, both at Palearctic latitudes (Vickers *et al.*, 2019) and paleoplateau altitudes (Rodríguez-López *et al.*, 2022), and with more changing paleoclimates, also in Iberia (*e.g.* Hay and Floegel, 2012; Laita *et al.*, 2020, 2021). The recent discovery of Hauterivian glacial deposits in the Cameros Basin (northern Iberia) (Rodríguez-López *et al.*, 2024), together with recent paleogeographic reconstructions (*e.g.* King *et al.*, 2021; Rosembaum *et al.*, 2002; Tugend *et al.*, 2015; Vissers and Meijers, 2012) and the high estimated inclinations (55-60º) of the Valanginian-Barremian magnetic vector in the Lusitanian Basin (Moreau *et al.*, 1997) and the Pyrenean Organyà Basin (Gong *et al.*, 2008), point to a latitude of up to 42-50ºN for Iberia during the Early Cretaceous, which lies within the temperate climatic zone.

METHODS

The carbonate interval of the El Castellar Formation (129m) was logged bed by bed at a 1:100 scale in the

Castillo de Aliaga section (40º40'37"N and 0º42'26"W). This logging sough to characterize facies and facies trends and to identify high-frequency sequences (Fig. 1B). Given the abundant metric- to hectometric-scale faults with metric to decametric offsets, the outcrop was studied to analyze fault displacements. A detailed aerial orthoimage (1:5000) was also used for this purpose (Fig. 1C). As a result, the section was logged with lateral displacement along the outcrop to ensure a continuous record and prevent repetition. The field study involved describing and documenting the lithology, sedimentary facies, sedimentary structures, and fossil content using standard field tools. Each meter of the section was marked in the outcrop (using markers or paint) to facilitate subsequent observations. During the logging process, 146 samples were collected, comprising 98 rock samples and 48 sediment samples, with at least one sample taken per meter of the section to aid in the comprehensive description of the sedimentary facies and fossil identification. From the collected samples, 98 polished sections and 64 selected thin sections (30μm thick) of rocks were produced and studied using a binocular loupe and a polarizing petrographic microscope with camera (model OPO 185, KERN Optics). High-resolution images were also captured with an Epson V100 photo scanner (model J231B) and a Plustek OpticFilm scanner (model 8300iSE). Sediment samples were levigated using a sieve shaker machine with 1000, 500 and 100μm mesh openings, and the residue was examined with a binocular loupe.

The concept of high-frequency sequences of different scales is used here from a descriptive perspective, implying a hierarchical organization where smaller sequences are nested within larger ones (*e.g.* Mitchum and Van Wagoner, 1991). The identification of these sequences, including elementary sequences, parasequences, and parasequence sets, relies on recognizing discontinuity surfaces that indicate breaks in sedimentation and/or vertical facies trends within sequences (*e.g.* Bosence *et al.*, 2009; Sevillano *et al.*, 2020). The lacustrine sequences at different scales mainly correspond to shallowing-upward successions, with features of exposure (oxidation, brecciation and root bioturbation) toward the top of the sequences. The time frame for each sequence type is based on the cyclostratigraphy from Illueca *et al.* (2023), who undertook a spectral analysis of the time series (depth domain) of the magnetic susceptibility and lithological data (data every 0.5m) of the stratigraphic section studied here. Smoothed curves for significant periodicities (95kyr and 22.4kyr cycles) were obtained by applying a Gaussian filter using PAST software (Hammer *et al.*, 2001). The analysis of variations in accommodation over time, following Schwarzacher (2005), involved constructing a graph of accumulated thickness deviations for each stratigraphic sequence or cycle in relation to their respective average thicknesses.

RESULTS

The Castillo de Aliaga section

The strata of the El Castellar Formation in the Castillo de Aliaga section exhibit NW-SE to E-W strikes and high dips toward the NE and N. Numerous faults, ranging from meter- to hectometer-scale, cut through strata, resulting in thickness variations in discrete beds of a clearly synsedimentary character (Fig. 1C). The logged section includes three different lithological groups (stratigraphic sections I, II, and III in Fig. 2). The lowest section (I) is 27m thick and mainly consists of limestone with a few marl beds. The middle section (II), which is 42m thick, is dominated by variegated marls and clays with a much lower proportion of limestone. Finally, the upper section (III) is 58m thick and mainly consists of a succession of marl, marlstone and limestone.

The El Castellar Formation is made up of decimeter- to meter-thick tabular strata of marl, marlstone, marly limestone, and limestone, varying in predominance throughout the unit (Fig. 2). Claystone is present to a lesser extent. Occasionally, more detrital beds, such as silts, fine sands, or conglomerates, and mixed siliciclastic-carbonate lithologies (silty/sandy marls and limestones) are intercalated. The limestones and marlstones frequently display oxidation (Fe oxides), bioturbation and brecciation, especially near the top of the beds. The limestones are mainly mudstones and wackestones, with some packstones present. Sedimentary structures such as parallel and cross-lamination, cross-bedding, and symmetric or asymmetric ripples are common in the upper part of the section. The marls are mostly green and gray, and are usually massive and sometimes laminated. The clays are also massive and exhibit a range of colors, including red, violet, ocher and gray. The fossil content is abundant, with a predominance of charophytes (oogonia and stalks), along with bivalve fragments, ostracods, and scarce gastropods and fish teeth.

Facies associations

Nine lacustrine facies associations are distinguished (Fig. 3): Low-Energy Shallow Lake (LESL)-1 and LESL-2; Mixed Siliciclastic-Carbonate Lake (MSCL)-1, MSCL-2, and MSCL-3 and High-Energy Lake (HEL)-1, HEL-2, HEL-3 and HEL-4.

The LESL facies associations are made up of limestone sequences occasionally found overlying marls and clastic sequences. The limestone evolves from micritic mudstone or wackestone to bioclastic packstone, typically ending with features of subaerial exposure such as brecciation, oxidation, and/or bioturbation.

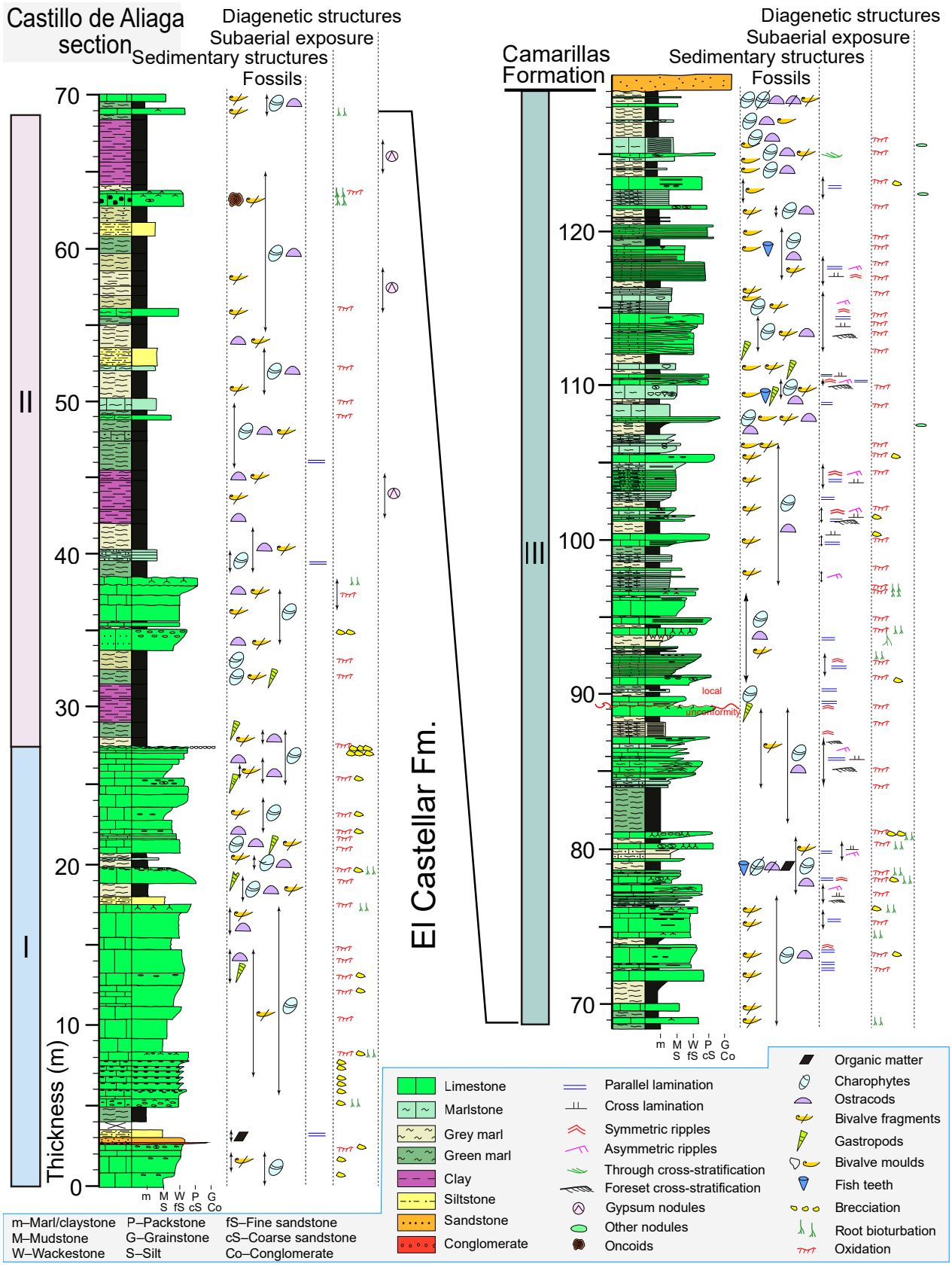

FIGURE 2. The El Castellar Formation in the Castillo de Aliaga section. Lithologic and textural log including the sedimentary structures, fossil content, subaerial exposure features, and diagenetic structures, as well as the three different stratigraphic sections (I, II and III) identified in the studied section.

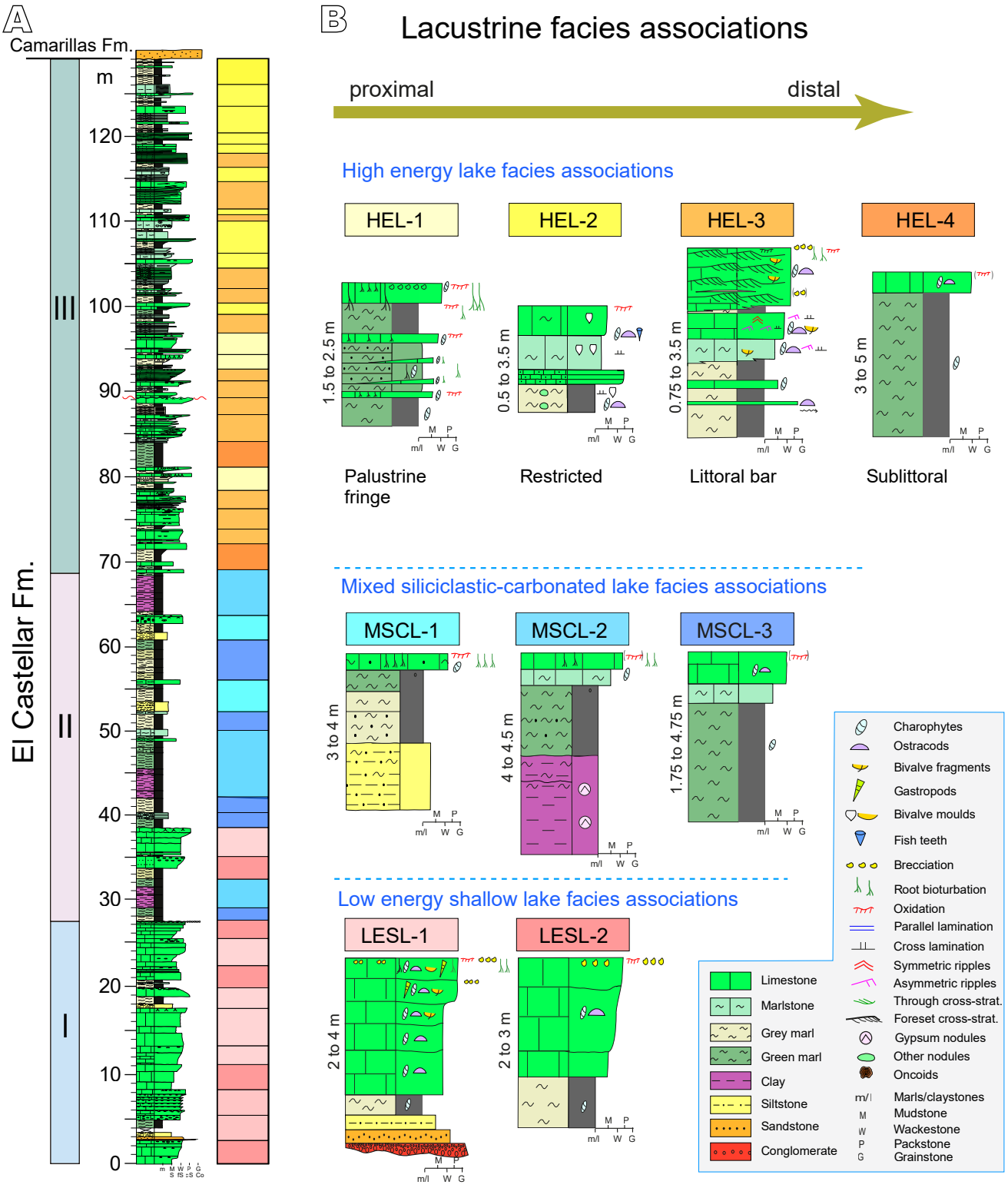

FIGURE 3. Facies associations of the lacustrine El Castellar Formation in the Castillo de Aliaga section. A) Distribution of facies associations in the stratigraphic log. B) Ideal stratigraphical sections of the facies associations recognized in the lake system, from proximal to distal areas, evolving over time from a Low-Energy Shallow Lake (LESL), through a Mixed Siliciclastic-Carbonate Lake (MSCL), to a High-Energy Lake (HEL).

LESL-1 is made up of facies sequences from 2 to 4m thick and mainly comprises limestones (Fig. 3B). When present, the marl is gray to green and forms massive, dm-scale tabular beds containing abundant ostracods and charophytes. Occasionally, a lower siliciclastic term occurs, featuring a fining-upward sequence that includes a cm-thick conglomerate with lenticular geometry and homometric, sub-rounded calcareous pebbles, a dm-thick fine-grained sandstone, and a gray tabular silt with parallel lamination. The upper limestones consist of dm- to m-thick tabular beds of mudstone-wackestone textures with charophytes, ostracods, and bivalve fragments (Fig. 4A), transitioning to wackestone to wackestone-packstone textures and occasionally packstones with charophytes (Fig. 4B-C), ostracods, bivalve fragments, and fewer gastropods. The preservation of the fossils is generally good, although some fossils may be fragmented. The tops of these limestone sequences frequently show evidence of subaerial exposure, including oxidation (Fe oxides), but also root bioturbation or brecciation (Fig. 4D). This facies succession mainly occurs in the lower section (I) and occasionally in the middle section (II) of the stratigraphic profile and is vertically related to the LESL-2 facies association (Fig. 3A).

LESL-2 consists of 2 to 3m-thick successions of limestones that often overlie dm- to m-scale tabular beds of massive gray to green marls containing abundant ostracods and charophytes. The limestones are dark gray, occur in dm-thick tabular layers, and range from mudstone to wackestone or wackestone-packstone, containing charophytes, bivalve fragments, ostracods, and gastropods (Fig. 3B). The preservation of fossils, especially of charophytes, can be exceptional (Fig. 4E). At the top of the sequences, these limestones occasionally show features of subaerial exposure such as brecciation and oxidation surfaces (Fig. 4F), but without root bioturbation. This facies succession is particularly prevalent in the lower section (I) and occasionally in the middle section (II) of the stratigraphic profile and is related to the LESL-1 and MSCL-3 facies associations (Fig. 3A).

The MSCL facies associations are characterized by mixed siliciclastic and carbonate facies. There is a gradual increase in carbonate content from clays or silts at the base to marls, marlstones, and occasionally limestones at the top, with possible intermediate stages of sandy or silty marls (Fig. 5A). Generally, the marls, marlstones, and limestones also contain a high proportion of terrigenous material.

MSCL-1 forms 3-4m-thick successions that consist of up to 1.5m of massive silts, sandy or silty marls (both with scarce fossil content), and mudstone-wackestone to wackestone-packstone limestones arranged in dm-thick tabular beds, with bivalve fragments, charophytes and ostracods, and locally oncoids (Figs. 3B; 5A, B). The limestone also exhibits sedimentary features such as brecciation, bioturbation, and oxidation at the top of the beds (Fig. 5D-E). This facies association is identified in the middle part (II) of the section and is vertically related to the MSCL-2 and MSCL-3 facies associations.

MSCL-2 forms 3-4m-thick successions that begin with massive clays, which are red and versicolored on the surface and greenish to greenish-gray in fresh section. These clays often contain displaceable, isolated crystals or aggregates of gypsum, ranging from millimeters to centimeters in size, which are transparent or white (red on the surface). The sequence then transitions to sandy marls, clayey-marls, and finally, marlstones (Fig. 5C) or to charophyte wackestone-packstone limestones, with less oxidation and bioturbation at the top of the beds. This facies association is identified in the middle part (II) of the section and is vertically related to the LESL-2, MSCL-1, and MSCL-3 facies associations.

MSCL-3 consists of m-thick sequences of marl, marlstone, and limestone, with marl being the main lithology (Fig. 2C). The marl and marlstone are green and gray, rich in charophytes and less abundant in ostracods, and are present as massive and sometimes laminated tabular bodies on a meter to decimeter scale. The limestone is gray and exhibits mudstone and wackestone textures with charophytes and ostracods, and is arranged in dm-thick tabular beds. Evidence of subaerial exposure is rare, with only occasional oxidation. This facies association is identified in the middle part (II) of the section and is vertically related to the LESL-1, LESL-2, and especially to the MSCL-1 and MSCL-2 facies associations.

The HEL facies associations consist of a succession of marls, marlstones, and slabby limestones, frequently exhibiting cross-bedding, internal lamination, and ripples (Figs. 3B; 6). Charophytes are the predominant fossils, accompanied by ostracods and bivalves. In general, the fossils are more fragmented and less well preserved than in the LESL facies associations, with wackestone and packstone textures being common (Fig. 6B-C). Features of subaerial exposure are also common at the top of the limestone beds.

HEL-1 consists of 1.5-2.5m-thick successions of green marls, sandy marlstones, and decimeter-thick beds of mudstone to wackestone with charophytes and ostracods (Fig. 3B). Centimeter- to decimeter-thick layers of charophyte mudstone-wackestone are intercalated within the marl. Early diagenetic processes are particularly intense, evidenced by strong mottling due to oxidation, brecciation in the upper parts of the sequences, and especially root bioturbation, which is abundant across all the limestone facies, with roots penetrating deep (up to 20-30cm) into the marls (Fig. 6D). This facies association is located in the

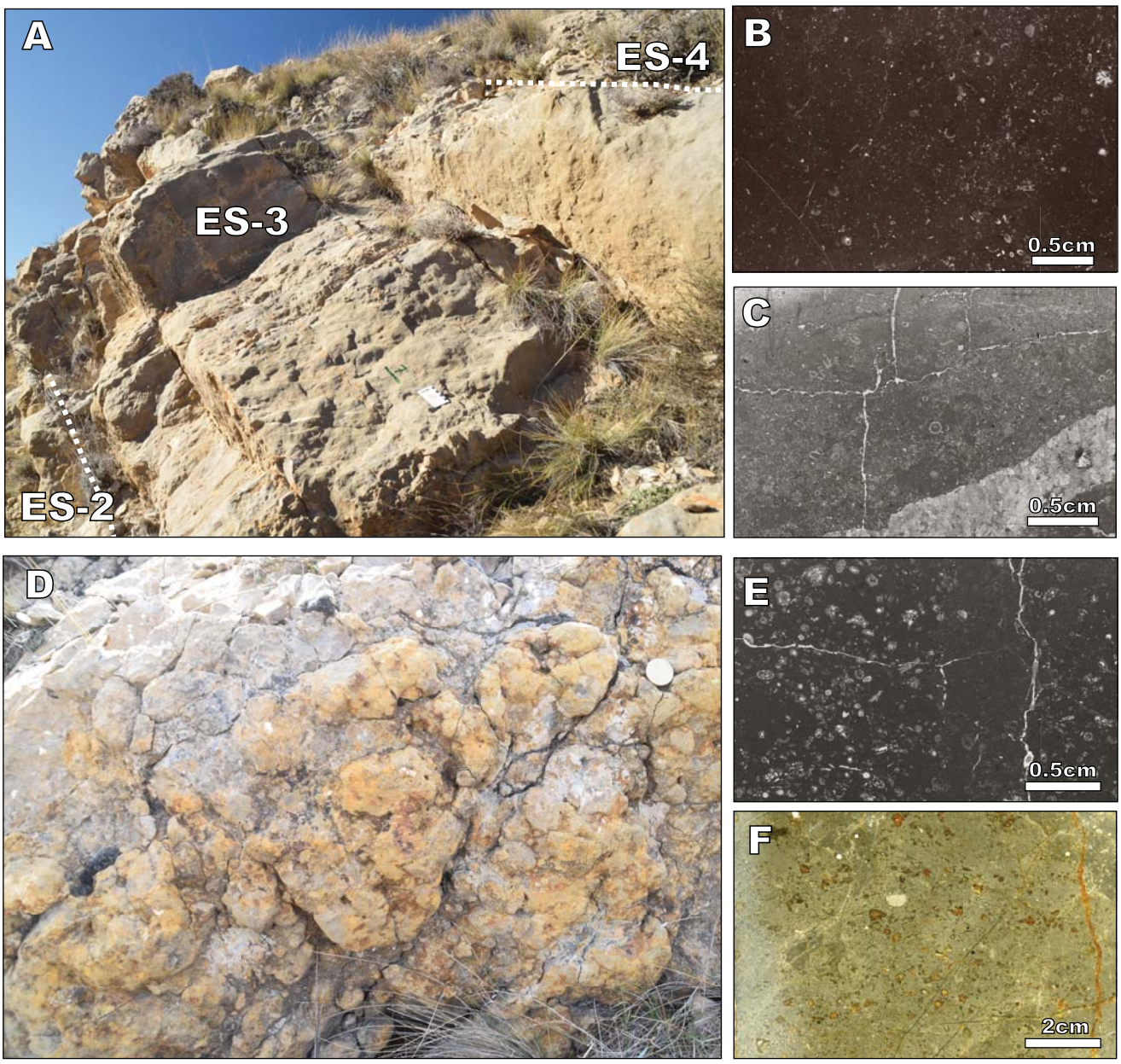

FIGURE 4. Low-Energy Shallow Lake (LESL) facies association. A) Field view of the charophyte mudstone-wackestone of LESL-1 facies association (elementary sequence ES-3). B) Thin section (parallel nicols) of mudstone-wackestone facies (LESL-1). C) Thin section (parallel nicols) of packstone facies (uppermost of LESL-1). D) Field view of limestones at the top of the LESL-1 facies association showing root bioturbation, oxidation and brecciation. E) Thin section (parallel nicols) of wackestone facies of LESL-2, with a good preservation of charophyte stems and oogonia (upper left corner). F) Polished section of a wackestone-packstone limestone from an upper level of LESL2, with oxidation and brecciation.

lower part of stratigraphic section III, where it is vertically related to HEL-3 and HEL-4 (Fig. 3A).

HEL-2 typically consists of a succession up to 3.5m thick of gray marls, marlstones, and limestones (Fig. 3B). The marls, up to dm-thick, are massive, contain charophytes and ostracods, and occasionally exhibit nodulization at the top. The marlstones, also up to dm-thick, are laminated, contain charophytes, ostracods, and bivalve fragments, and occasionally display nodulization as well. Some beds have molds of entire large bivalves (articulated and disarticulated). Locally, there are cm- to dm-thick tabular layers of highly oxidized calcareous sandstones with bivalve molds. The limestones of HEL-2 are micritic, ranging from mudstone to mudstone-wackestone, with charophytes and ostracods, and abundant molds of entire bivalves (Fig. 6E), along with occasional fish teeth. These limestone beds often have oxidized (Fe oxides) tops. HEL-2 is situated

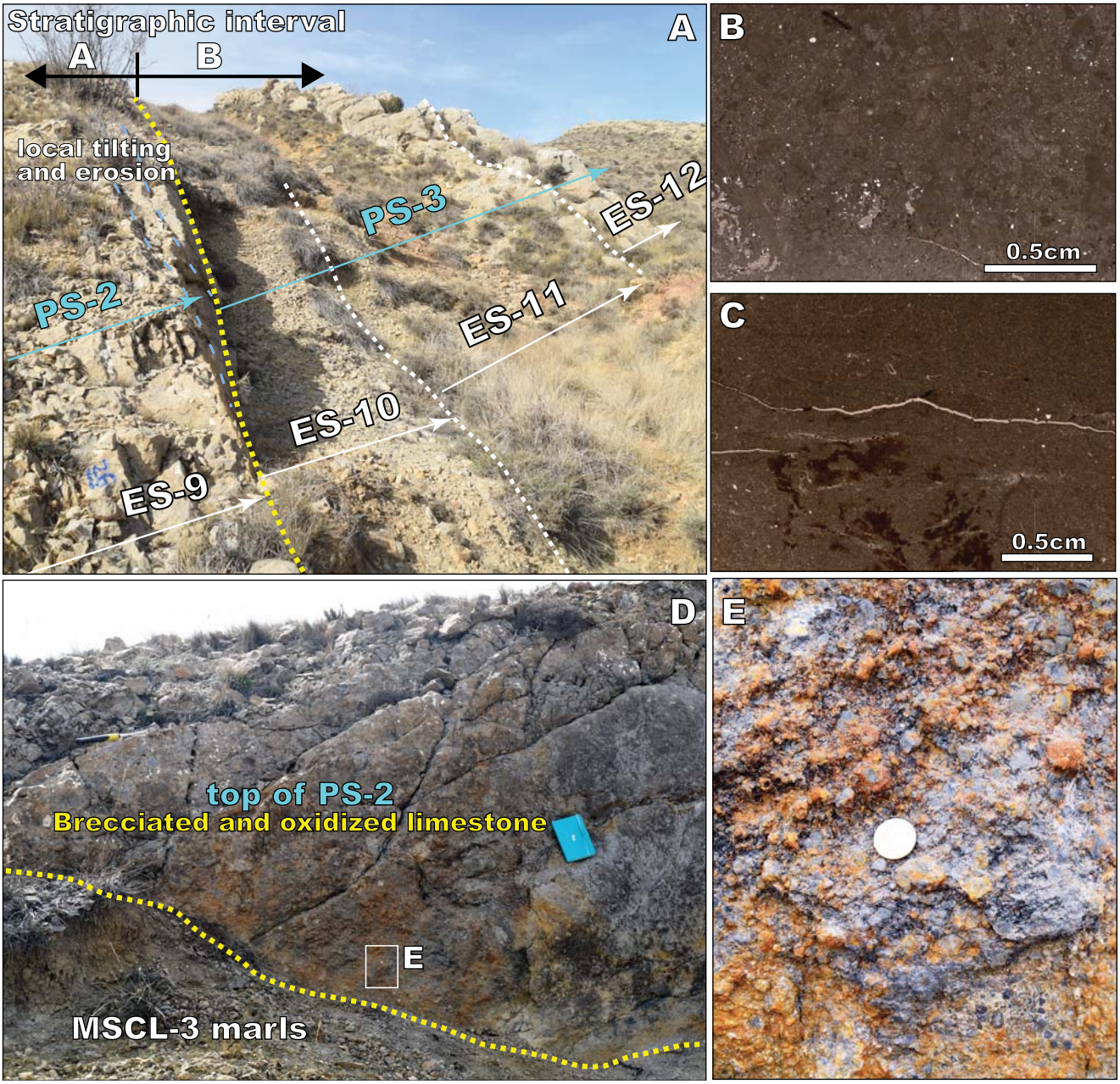

FIGURE 5. Mixed siliciclastic-carbonate lake (MSCL) facies associations. A) Field view of elementary sequences and parasequences at the boundary between stratigraphic sections I and II. Yellow dashed line shows the boundary between parasequence sets SPS-1 and SPS-2 (PS-2–PS-3 boundary). Note the local tilting and erosion of underlaying PS-2 parasequence. B) Thin section (parallel nicols) of an oncolytic limestone (MSCL-1). C) Thin section (parallel nicols) of marlstone (upper term of MSCL-2). D) Field view of the stratigraphic surface of the boundary between the PS-2 and PS-3 parasequences, also the boundary between SPS-1 and SPS-2 (see location in Fig. 5A), showing the significant subaerial exposure, with oxidation, brecciation, and bioturbation. E) Detail of brecciated and oxidized facies shown in D.

in the upper half of stratigraphic section III, where it is vertically related to HEL-3 (Fig. 3A).

HEL-3 forms sequences up to 3.5m thick, consisting of a succession of gray to green marls, marlstones, marly limestones, and bioclastic limestones (Fig. 3B). The marls, arranged in dm-thick tabular beds, are massive or laminated and contain abundant charophytes and ostracods. Locally, they intercalate with cm-thick beds with wackestone-packstone textures containing charophytes and ostracods. The marlstones and marly limestones contain charophytes, ostracods, and bivalve fragments, and are arranged in dm-thick beds, generally laminated and rarely massive. They are sometimes oxidized and may present ripples, with intercalated cm-thick layers of bioclastic packstone. The limestones, which are

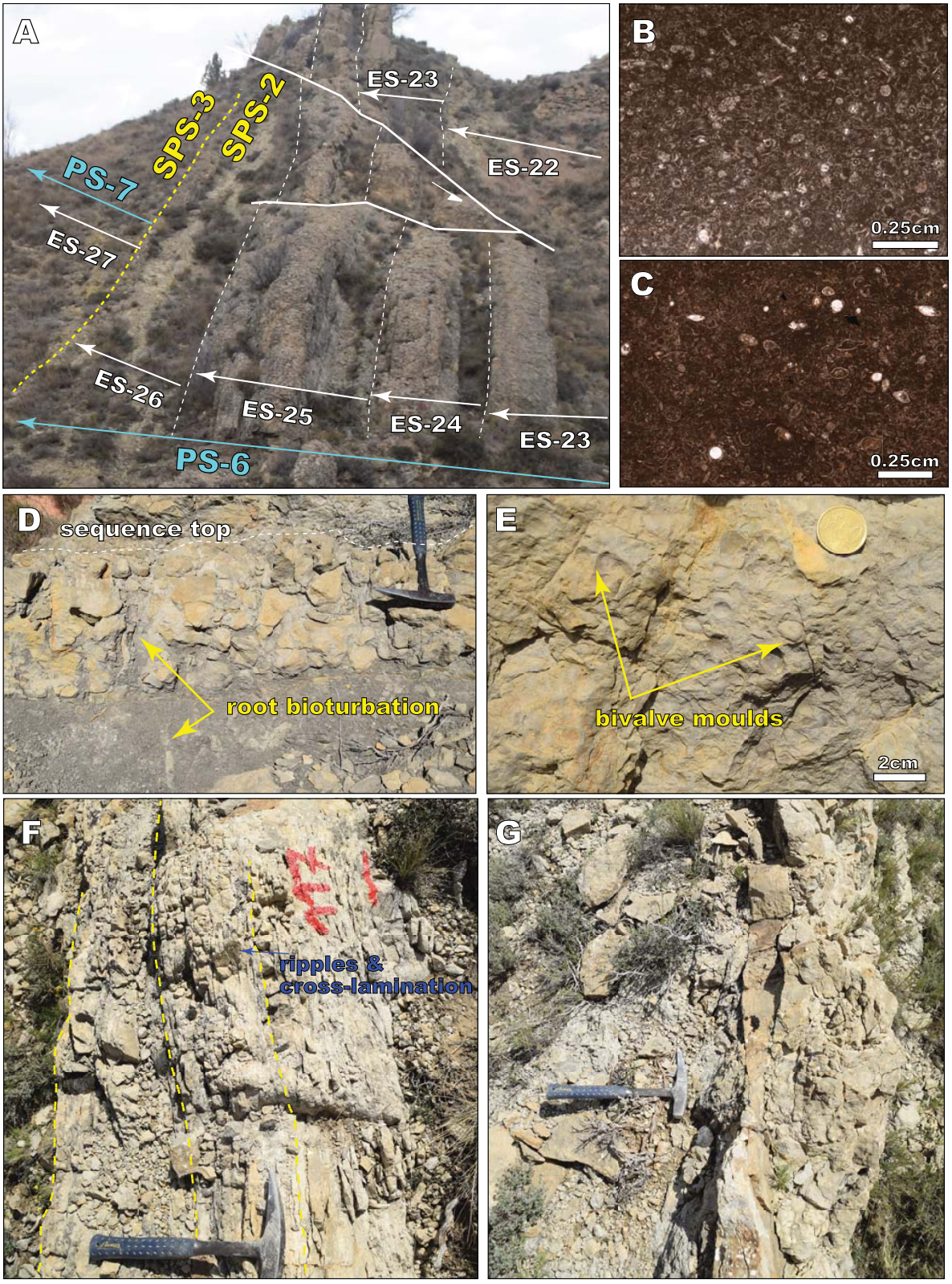

FIGURE 6. High-Energy Lake (HEL) facies associations. A) Field view of elementary sequences and parasequences of the base of stratigraphic section III and the boundary between SPS-2 and SPS-3 (dashed yellow line). B) and C) Thin sections (parallel nicols) show charophyte packstone facies from the HEL facies association, with occasional ostracods. D) Field view of palustrine HEL-1 facies, characterized by highly oxidized limestones with vertical root bioturbation extending into the marl. E) Field view of the limestones term of HEL-2 facies association, containing abundant entire bivalve moulds. F) and G) Field views of high-energy littoral bar facies from the HEL-3 facies association, exhibiting lamination, ripples, and cross-bedding.

occasionally silty, are mainly bioclastic wackestones and packstones, with abundant charophytes, ostracods, bivalve fragments, and a lower content of gastropods (Fig. 6B-C). These limestones are frequently laminated or slabby and are arranged in decimeter- to meter- thick tabular bundles, exhibiting internal cross-lamination and current or oscillation ripples (Fig. 6F). Toward the top, they often show signs of oxidation and bioturbation, mainly vertical root traces, and occasionally horizontal bioturbation, with less frequent brecciation. The sequence ends with dm- to m-thick tabular beds of bioclastic limestones, ranging from wackestone to packstone with charophytes, ostracods, and bivalves, which may intercalate with cm-thick marl beds. The facies are intensely laminated and slabby, with dm-scale cross-stratification and abundant ripples (Fig. 6G). The limestones also show frequent oxidation, bioturbation, or brecciation on their upper surfaces. Facies association HEL-3 is located in the lower half of stratigraphic section III and is vertically related to HEL-2, as well as to HEL-1 and HEL-4 (Fig. 3A).

HEL-4 consists of a thick lower unit (3 to 5m thick) of green massive marls with charophytes, and a thin bed of limestone (wackestone) with charophytes, ostracods, and bivalve fragments, showing some oxidation at the top (Fig. 3B). Facies association HEL-4 is located at the base of stratigraphic section III and is vertically related to MSCL-2, HEL-1 and HEL-3 (Fig. 3A).

Interpretation of the facies associations and sedimentary systems

The nine lacustrine facies associations that are distinguished are interpreted as representing deposition in three different lake systems that evolved over time (Fig. 3): a LESL, MSCL and HEL.

Low-Energy Shallow Lake (LESL)

The facies characteristics and vertical relationships of the LESL facies associations indicate that they represent low-energy, shallowing lacustrine sequences interrupted by occasional, more pronounced deepening events (Fig. 3B). These sequences were the result of the progressive infilling of a very shallow, hard water lake where charophytes were the main carbonate source, under conditions similar to those described by Murphy and Wilkinson (1980). LESL-1 and LESL-2 correspond to progressively more distal carbonate facies (Fig. 3B). In this context, the marl lithology represents sediment settling in the more distal parts of the lake system, whereas the micritic carbonate facies (mudstone and wackestone) suggest deposition under low-energy conditions in the proximal littoral or sublittoral areas. The charophyte and ostracod packstone facies, containing fragments of bivalves and gastropods, are indicative of deposition in littoral zones during more energetic episodes. These episodes, likely associated with storms or floods, would have caused the fragmentation and accumulation of bioclasts and introduced sediments from the distal alluvial-fluvial system. This process contributed to the formation of cm-thick conglomerates, fine-grained sandstones, and laminated silts in the littoral lacustrine areas.

The LESL facies associations correspond to sequences of infilling in the low-gradient margins of a shallow, poorly developed lake (Platt and Wright, 1991). The predominance of mudstone/wackestone, the good preservation of fossils, and the absence of wave or current structures suggest that these were isolated hard water lakes with low-energy margins. In such environments, the thickest accumulation of carbonate occurs in littoral areas due to the high productivity of benthic organisms (Platt and Wright, 1991; Alonso Zarza *et al.*, 2006; Meléndez *et al.*, 2009). These lakes are highly sensitive to minor fluctuations in lake level, which can lead to subaerial exposure of more proximal deposits and the development of palustrine-type facies, such as oxidized, brecciated, or bioturbated limestones (Alonso Zarza and Wright, 2010). However, the extent of subaerial exposure is relatively limited (see the exposure index given by Platt and Wright, 1992), indicating a stable system with minimal sedimentary interruptions or erosive episodes. Consequently, features such as paleosols, microkarsts or calcretes are absent (Alonso Zarza and Wright, 2010; Luzón *et al.*, 2002).

Mixed Siliciclastic-Carbonate Lake (MSCL)

The three distinct facies associations that are identified represent deposition in different settings within a mixed siliciclastic-carbonate lacustrine system (Fig. 3B): proximal (MSCL-1), intermediate (MSCL-2), and distal (MSCL-3). This lacustrine system mainly occurs in the middle part (section II) of the stratigraphic profile and the distinct facies associations exhibit a vertical relationship with one another (Fig. 3A).

The MSCL facies associations are interpreted as shallowing-upward lacustrine sequences, with an increasing carbonate content in a lake environment characterized by higher siliciclastic input and/or lower carbonate production. During periods of high sediment supply to the lake, terrigenous facies (silts and sandy marls) were mainly deposited in the proximal areas of the lacustrine system (MSCL-1), whereas clays settled by decantation in the intermediate areas (MSCL-2). In the central parts of the lake, further from the terrigenous sources, marl deposition dominated (MSCL-3). As the sediment supply diminished, carbonate production within the lake resumed, leading to the deposition of marls, followed by limestones, in both the

marginal and central lake areas. Accordingly, this sequence reflects a progressive decrease in terrigenous input to the lake. The proportions of limestone relative to marl, along with the indicators of subaerial exposure (such as oxidation and bioturbation) in the limestones at the top of the lacustrine sequences, are greater in the proximal areas (MSCL-1) than in the intermediate (MSCL-2) and distal areas (MSCL-3) of the lake. The gypsum crystals found in the massive greenish-gray clays of MSCL-2, as suggested by Liesa *et al.*(2006), are interpreted as late diagenetic in origin, having formed in sediments saturated with highly mineralized water.

High-Energy Lake (HEL)

The four identified HEL facies associations characterize a high-energy lake system (Fig. 3B), which occurs predominantly in the upper part (section III) of the stratigraphic profile (Figs. 3A; 6A).

The HEL facies associations represent deposition in different subenvironments within this lake system (Fig. 3B), ranging from the palustrine fringe (HEL-1), through the high-energy littoral bar (HEL-3), to the sublittoral environment (HEL-4). HEL-2 reflects sedimentation in restricted areas protected by the littoral bar. HEL-1 is interpreted as deposition in a low-gradient palustrine belt characterized by vegetated marshes or ponds, where marls and limestones formed and where the vegetation bioturbated and mottled the sediments. The sandy facies are attributed to detrital inputs from alluvial flows entering the palustrine belt. This facies association constitutes a marginal upward-shallowing sequence, in which the palustrine area gradually expands until the sediments are fully exposed, leading to the development of paleosols during prolonged periods of vegetation colonization. HEL-2 is interpreted as having formed under low-energy conditions in restricted and protected areas where mud facies were deposited, giving rise to significant accumulations and preservation of bivalves, along with some siliciclastic inputs from nearby areas. HEL-3 corresponds to the progradational sequence of a lacustrine littoral bar that developed in high-energy settings. Massive or laminated marls and thin layers of tabular (sometimes laminated) bioclastic limestone represent bottomset deposits, whereas dm-scale cross-bedded bioclastic limestones correspond to the foreset migration of bioclastic bars with superimposed ripples, which developed in high-energy lake environments. Finally, HEL-4 represents the most distal facies associated with this high-energy system, characterized by thick deposits of marls that reflect the settling of suspended sediments in more central lacustrine areas. The few limestones at the top of the sequences, showing local subaerial exposure, represent sedimentation during periods of low lake levels, indicating a shallowing upward sequence very similar to those in the low-energy systems (*i.e.* MSCL-3).

The HEL facies associations are interpreted as representing lacustrine sedimentation in a shallow, extensive, high-energy, low-gradient (ramp-type) lake (Platt and Wright, 1991). Large-scale bars and ripples would have developed in littoral zones under high-energy conditions characterized by currents and wave action, as described in other lake systems from the Lower Cretaceous of the Iberian Basin (Fregenal-Martínez and Meléndez, 2000; Meléndez *et al.*, 2000). Fluctuations in lake level would have controlled the deposition and stacking of different sequences, such as the superimposition of palustrine environments over lacustrine ones, or the sudden deepening of the system. Therefore, this HEL system, although more developed and extensive than the systems described above, would have still been a shallow lake sensitive to these oscillations in water level, often undergoing subaerial exposure and root bioturbation during periods of low lake level.

High-frequency sequences

The analysis of bounding surfaces and facies trends makes it possible to recognize hierarchically stacked stratigraphic sequences at three distinct scales within the lacustrine evolution of the El Castellar Formation (Fig. 7A-B): the Elementary Sequence (ES), the parasequence (PS), and the Set of Parasequences (SPS).

Elementary Sequences (ES) are high-frequency, small-scale sequences with an average thickness of ~2.91m (ranging from 1.25 to 5.25m; mode: 2.75-3.24m) (Fig. 8A). A total of 44 elementary sequences (ES-1 to ES-44) are identified (Fig. 7B). The ESs are bounded by distinct surfaces, typically characterized by a sudden deepening of the lacustrine facies that overlie the shallower facies of the preceding elementary sequence. These previous facies often exhibit features of subaerial exposure, such as brecciation, oxidation, and/or root bioturbation. Differentiating elementary sequences in distal facies composed of marls and clays is challenging, so some sequence boundaries are defined tentatively (ES-16 to ES-17). ESs mainly correspond to the facies associations described in the previous section, representing sequences of shallowing lacustrine settings.

Parasequences (PS) are medium-scale, high-frequency sequences with an average thickness of ~12.4m (ranging from 9.75 to 17.5m) (Fig. 8B). A total of ten complete parasequences (PS-1 to PS-10) and two incomplete ones (PS-0 and PS-11) are recognized (Fig. 7B). The complete parasequences typically consist of four elementary sequences (PS-1, PS-2, PS-3, PS-5, PS-8, PS-9, PS-10, and probably PS-4) or occasionally five (PS-6 and PS-7), with

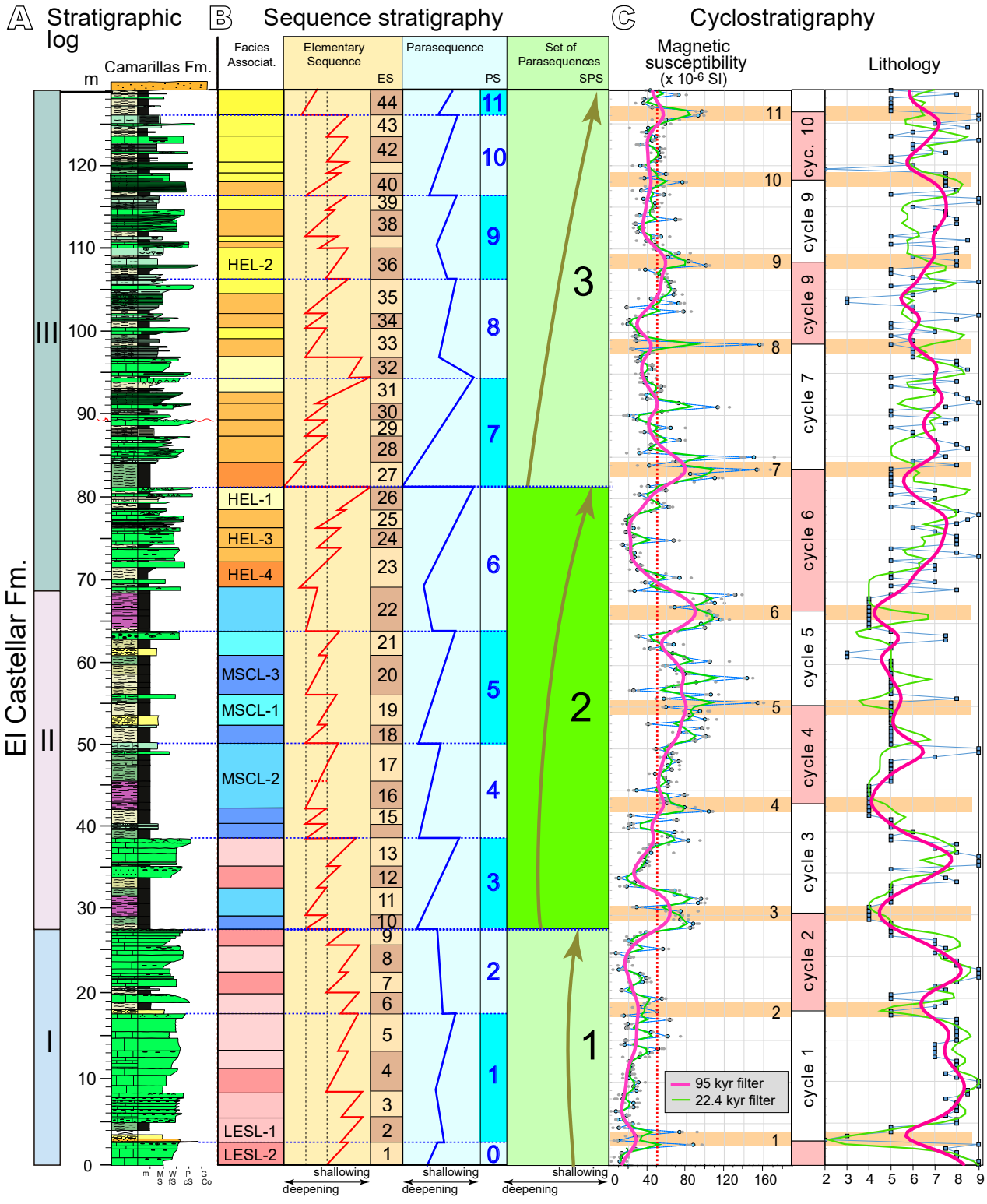

FIGURE 7. Linking high-frequency sequences of different orders with orbitally induced cyclicity in the lacustrine El Castellar Formation. A) Stratigraphic record. B) Facies associations and high-frequency sequences of small (elementary sequences), medium (parasequences) and large scale (sets of parasequences) recognized and their vertical facies trend (sequences numbered in correlative order). C) Raw and smoothed curves from cyclostratigraphic time series data, including Magnetic Susceptibility (MS) and lithology, as well as the 95kyr cycles identified in the stratigraphic section (after Illueca et al., 2023). Smoothing was carried out using a 25 data (12.5m) or 6 data (3m) Gaussian filter for the 95kyr and 22.4kyr filter, respectively. Note the inverse correlation between the two curves and the eleven maxima in the 95kyr MS filter (orange bands), which Illueca et al. (2023) used to identify ten complete and two incomplete cycles throughout the profile.

an average of 4.2 ESs per PS. Their thickness generally increases from PS-2 to PS-6 and then progressively decreases. The parasequence boundaries are marked by clear stratification surfaces defined by sharp lithological changes, corresponding to deeper facies overlying the shallower facies of the previous parasequence, often exhibiting signs of subaerial exposure (such as brecciation, oxidation, and/or root bioturbation). Most parasequences show a vertical progradational evolution, characterized by a shallowing-upward trend (PS-3 to PS-7 and PS-10). However, some show a significant aggradational component with a relatively progressive deepening at the base of the parasequence (PS-1, PS-2, PS-8, and PS-9) (Fig. 7B). The shallowing-upward trend is represented by the succession of distal LESL-2 and proximal LESL-1 facies (PS-1 and PS-2) in the LESL (stratigraphic section I); by the succession, whether complete or incomplete, of distal carbonate (MSCL-3), distal mixed (MSCL-2), and proximal mixed (MSCL-1) facies (PS-4 and PS-5), and locally of LESL-2 and LESL-1 (PS-3), in the MSCL (section II); and by the succession of sublittoral (HEL-4), littoral bar (HEL-3) and palustrine (HEL-1) facies (PS-6 and PS-7) or the succession of littoral bar (HEL-3) and restricted area (HEL-2) facies (PS-8 to PS-10) in the HEL (section III).

Sets of Parasequences (SPS) are large-scale, high-frequency sequences each about 54m in thickness. Three SPSs are identified (SPS-1 to SPS-3), with SPS-1 being incomplete (Fig. 7B). These sets correspond to three distinct lithological sections bounded by key flooding surfaces. SPS-1, which is 27m thick and incomplete, includes two parasequences (PS-1 and PS-2) and is made up of limestone from the proximal areas of a low-energy lake system. SPS-2 marks the beginning of significant clastic supply and the development of a low-energy mixed siliciclastic-carbonate lake system. SPS-2 is 54m thick, comprises four stacked parasequences (PS-3 to PS-6), and is essentially composed of mixed siliciclastic-carbonate lake shales and marls. SPS-3 is 48m thick, includes four parasequences (PS-7 to PS-10) and the elementary sequence ES-44, and is mainly composed of limestone sedimented in a lacustrine littoral bar and proximal areas of a high-energy lacustrine system. SPS-3 marks the onset of sublittoral facies over the palustrine environments of SPS-2 in the high-energy lake system. Its upper limit is defined by a sharp change of facies from the El Castellar Formation to the fluvial deposits of the Camarillas Formation. The sedimentary evolution is aggradational for SPS-1 and shallowing for the two other sets, reflecting an evolution consistent with the individual parasequences within each set. It is worth noting that even though SPS-1, SPS-2, and SPS-3 correspond approximately to lithological groups I, II, and III (Fig. 7A-B), there are discrepancies. For example, SPS-2 extends up to meter 81 instead of 68.5 (the top of II) and includes parasequence PS-6. The upper limit of SPS-3 is based primarily on a significant flooding event, marked by the transition from sublittoral to palustrine facies.

DISCUSSION

Linking high-frequency lacustrine sequences to orbitally-forced ciclicity

The high-frequency sequences within the lacustrine El Castellar Formation mainly constitute shallowing-upward sequences, stacked hierarchically at different scales (elementary sequences, parasequences, and sets of parasequences). These stratigraphic units are characterized by clear bounding surfaces that indicate abrupt changes in sedimentation and facies trends. The boundaries between different sequence orders mainly correspond to lacustrine flooding surfaces, which often overlie shallower facies exhibiting signs of subaerial exposure such as brecciation, oxidation surfaces, and root bioturbation. The development of the sequences and their facies trend is closely linked to changes in lake levels driven by climatic variations that controlled the supply of water and clastics to the hard water lake, where bioinduced carbonate production occurred.

Furthermore, in our case study, these stratigraphic sequences of varying orders can be correlated with different orbital cycles. The average thickness of elementary sequences (~2.9m; range 1.25 to 5.25m), parasequences (~12.4m; range 9.75 to 17.5m), and sets of parasequences (~54m) in the lacustrine deposits (Fig. 8) corresponds closely to the main periodicities of ~3.3, ~13.2 and ~57.3m, respectively. These periodicities were inferred from the spectral analysis of the time series of the magnetic susceptibility and lithology of this same section of the El Castellar Formation (Illueca *et al.*, 2023) (Fig. 7C). Accordingly, these high-frequency lacustrine sequences can be linked to this cyclicity, which was driven by orbital parameters (Illueca *et al.*, 2023). The elementary sequences are thus associated with the cyclical climate control of sedimentation induced by the long precession cycle (22.4kyr), which affects the orientation of the Earth's rotation axis. Similarly, parasequences and sets of parasequences are sedimentary cycles forced respectively by the short (95kyr) and long (405kyr) cycles of the Earth's orbit around the Sun (Fig. 7B-C).

The link between high-frequency lacustrine sequences and orbitally forced cyclicity not only provides a temporal framework for the former but also offers an additional line of evidence for correlating sedimentary cycles and orbital cycles. This is achieved by examining the number of stacked sequences relative to the corresponding time frame. For instance, each parasequence (95kyr) comprises four elementary sequences (22.4kyr) in eight cases

and five in two cases, resulting in an average ratio of 4.2 elementary sequences per parasequence (Figs. 7; 8). This ratio aligns the time span of these medium- and small-scale high-frequency sequences with the expected relationship between the orbital cycles (4.24 precession cycles per short eccentricity cycle). Similarly, the sets of parasequences (405kyr) stack four parasequences (95kyr) in SPS-2, or four parasequences plus one elementary sequence in SPS-3, which also aligns with the ratio of 4.26 between the eccentricity orbital cycles.

An additional constraint can be established by comparing the lacustrine parasequences with the 95kyr cycles defined from the smoothed data curves (25 data points, 12.5m intervals) of the magnetic susceptibility and lithology data series (Fig. 7C). Illueca *et al.* (2023) used the maxima in magnetic susceptibility (and minima in lithology) in these smoothed curves as references to distinguish short eccentricity cycles (orange bars). They identified ten complete 95kyr cycles with an average thickness of 12.3m, which is nearly identical to the average thickness of the parasequences (12.4m) (Fig. 8A-C). The correlation between the parasequences and the cycles established from the smoothed curves is strong both in terms of the number of cycles and the distribution of their thicknesses (Fig. 7B-C). For instance, the thickest parasequence, PS-6, corresponds to the thickest cycle, cycle-6, whereas the thinner PS-9 and PS-10 align with the thinner cycle-9 and cycle-10, respectively.

However, the boundaries of the parasequences appear slightly out of phase with the magnetic susceptibility maxima used to define the 95kyr cycles (Illueca *et al.*, 2023), with only three instances where they practically coincide (PS-1, PS-2, and PS-10). Generally, the boundaries of the parasequences coincide with or are close to the inflection points of the curves. This is consistent with observations in the study of sequences and cyclic behavior, such as sequence stratigraphy (Christie-Blick, 1991; Posamentier and Vail, 1988; Wright and Marriott, 1993). In dynamic systems such as sedimentary environments, the inflection point marks the change in behavior, defining a sequence boundary (Simmons, 2016). In sequence stratigraphy, for example, bounding unconformities are related to the inflection points of eustatic falls (Posamentier and Vail, 1988), or boundaries of seismic sequences are located near the inflection points of eustatic sea-level fluctuations, where the rates of fall or rise are maximized (Jervey, 1988). The small observed mismatches may result from variations in the thickness of sedimentary sequences and from the analytical procedure itself, which may introduce minor errors during curve smoothing using a Gaussian filter.

Finally, the small-scale (elementary sequence) and medium-scale (parasequence) high-frequency lacustrine sequences, like the recorded long precession (22.4kyr) and short eccentricity (95kyr) cycles, exhibit variations in thickness over time within the stratigraphic series (Figs. 7; 8). These variations in thickness are comparable, which also highlights the link between high-frequency lacustrine sequences and climatically driven, orbitally induced cyclicity (Fig. 8).

Consequently, the high-frequency shallowing-upward sequences represent phases of lacustrine expansion and retraction caused by cyclic variations in orbital parameters, specifically the Earth's orbital eccentricity and precession cycles. These sequences may therefore be associated with climatic factors that correspond to changes in lake levels related to water supply, aridity, or variations in the water table (Bohacs *et al.*, 2000; Gierlowski-Kordesch *et al.*, 1991; Gómez-Fernández and Meléndez, 1994; Soria *et al.*, 2008, 2012). According to Morrill *et al.* (2001), orbital forcing can significantly impact the water balance of lake systems, especially in the absence of large salinity changes, as observed in our section. This impact is primarily driven by changes in lake evaporation and runoff coefficients, both of which are influenced by climatic factors such as short-wave radiation, temperature, and precipitation.

It is not clear how the effects of these orbital variations were transferred through the climate system and into the lacustrine sedimentary record (*e.g.* Morrill *et al.*, 2001; Ruddiman, 2006). Periods of tilt and precession force changes in insolation and greenhouse gases responsible for variations in climate and in the evolution of sedimentary systems. Despite negligible insolation forcing at the period of eccentricity, it has been suggested that the 100kyr periods are the result of internal resonance and feedback between the tilt and precession periods (Ruddiman, 2006). In our opinion, latitudinal variations in the climatic zones induced by orbital forcing cannot be ruled out, which may be responsible for cyclic sedimentary and climatic changes over long periods of time. This is particularly relevant for the study area, situated in a mid-latitude zone that may fall within the influence of either temperate or subtropical climatic belts. The paleogeographic changes in land and sea masses caused by the spreading of the southern North Atlantic during the Early Cretaceous (King *et al.*, 2021; Tugend *et al.*, 2015) could have also influenced regional climatic changes. Whatever the case, a detailed study of paleoclimatic proxies (*e.g.* conventional or clumped $\delta^{18}O$ and $\delta^{13}C$ carbonate isotopes) is necessary to characterize the relevance of these paleoclimatic changes, *i.e.* to resolve the question of whether the orbital cycles resulted in changes to the point of completely resetting the dominant climate, or whether some variables changed but the same climate persisted.

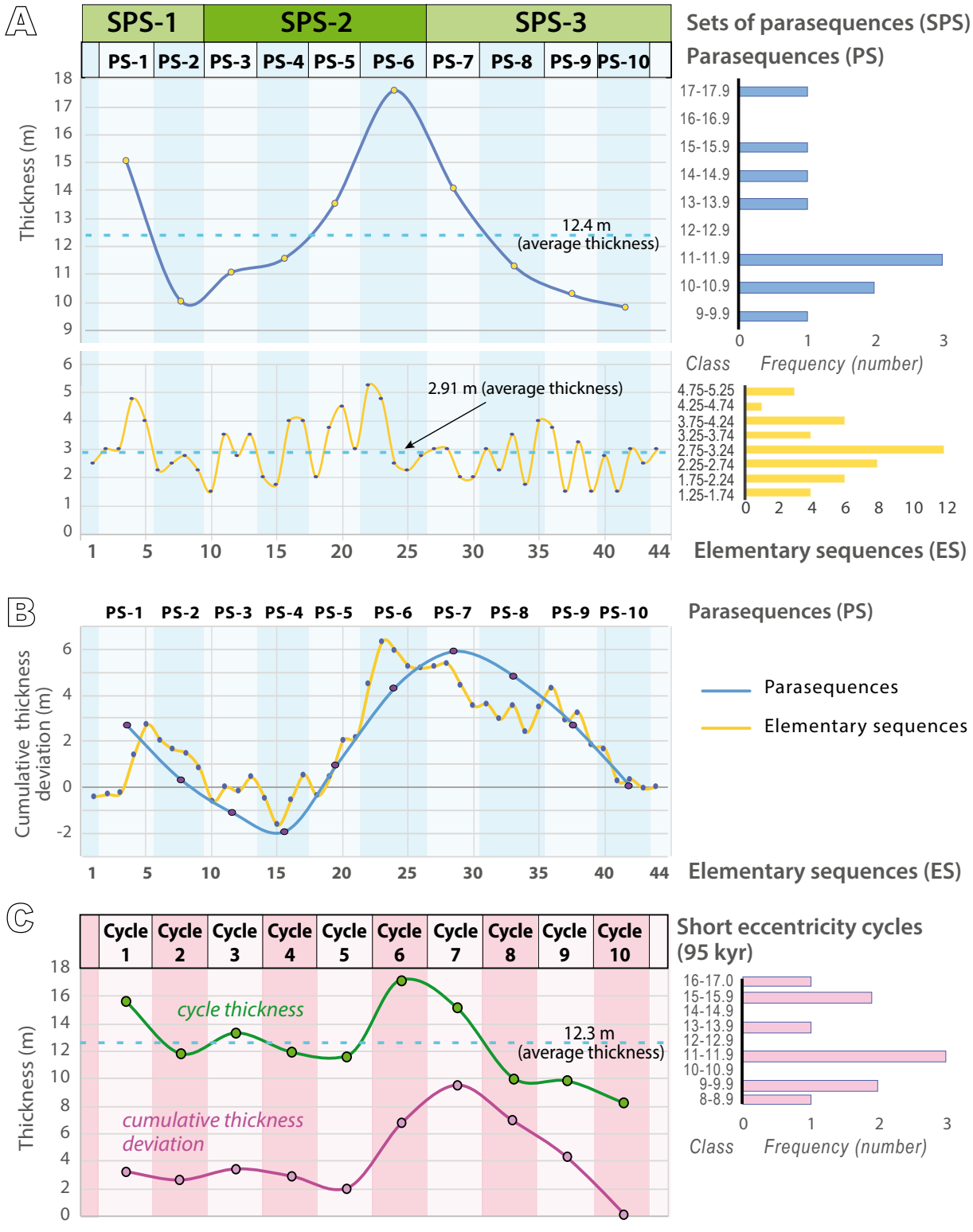

FIGURE 8. Analysis of thickness variation in high-frequency sequences, 95kyr cycles, and tectonic forcing on stacked sequences. A) Scatter plots and histograms illustrating the thicknesses of elementary sequences and parasequences, with the average thickness for each sequence type also indicated. B) Cumulative thickness deviation diagram (based on Schwarzacher, 2005; see methods) for elementary sequences and parasequences, depicting variations in the creation (mainly tectonic) of accommodation. In this graph, a drop in the curve indicates that the sequence/cycle is thinner than the average, while a rise indicates a thickness greater than the average. Thus, a positive slope indicates an increase in accommodation (accelerated tectonic subsidence), whereas a negative slope indicates a decrease (decelerated tectonic subsidence). C) Plots showing thickness and cumulative thickness deviation for short eccentricity cycles (95kyr) identified from the smoothed magnetic susceptibility curve (see Fig. 7C). Note the similarity among the different curves in relation to changes in thickness.

Tectonic control on sequence stacking

Changes in the thickness of sedimentary sequences and cyclicity of different temporal orders indicate changes in the rate of sediment accumulation over time (Fig. 8A-C). These variations in thickness within a synrift unit (Liesa *et al.*, 2004, 2006; Salas, 1987; Soria, 1997) are interpreted as having been strongly controlled by the generation of accommodation associated with tectonic processes, particularly tectonic subsidence. Variations in fault displacement likely caused changes in subsidence rates, thereby affecting the thickness of the recorded cycles, as also observed in other lacustrine systems (*e.g.* Casas *et al.*, 2024; Muñoz *et al.*, 2020; Soria *et al.*, 2012).

The creation of accommodation driven by tectonics is consistent with the significant faulting associated with the deposition of the El Castellar Formation in the Galve sub-basin (Aurell *et al.*, 2016; Liesa *et al.*, 2004, 2006, 2019; Meléndez *et al.*, 2009; Soria, 1997). Numerous normal faults in the study area displaced and altered the thickness of the sedimentary series (Fig. 1C). For example, the stratigraphic surface between SPS-1 and SPS-2 (the PS-2–PS-3 boundary) is marked by a major episode of subaerial exposure resulting from tilting and local erosion (Fig. 5A). Here, bed tilting was caused by the sliding of normal faults on a metric to decametric scale, which also led to the thickening of the clayey elementary sequences ES-10 and ES11 (Fig. 1C).

In this context, variations in the thickness of orbital cycles recorded in stratigraphic sequences can serve as a tool for analyzing tectonic activity associated with normal fault displacement. Such analysis relies on two key assumptions: first, that sediments fill the depositional space generated by fault displacement; and second, that most shallowing-upward lacustrine sequences culminate in facies indicating subaerial exposure, meaning the accommodation available was filled. Accordingly, the observed increase in parasequence thickness (and 95kyr cycles) from PS-2 to PS-6 (cycle 2 to cycle 6), followed by the progressive decrease until PS-10 (Fig. 8A-C), outlines a cycle of rising and then declining tectonic activity. This tectonic cycle spans approximately 30 elementary sequences (from ES-15 to ES-44), covering around 700kyr, which is comparable to certain tectonic cycles documented in the Teruel rift basin (Ezquerro, 2017; Ezquerro *et al.*, 2022b). Given the average thickness (without decompaction) of parasequences (12.4m) and elementary sequences (2.9m), along with their respective time spans (95 and 22.4kyr), the average accommodation rate in the lake system was 130m/Myr. However, the accommodation rate varied between 102 and 184m/Myr for different parasequences, and between 67 and 245m/Myr for elementary sequences. These values are typical of rift systems (Casas *et al.*, 2024; Ezquerro *et al.*, 2020; Friedmann and Burbank, 1995; Leeder, 1991).

The deviations in the accumulated thickness observed in each elementary sequence, parasequence (Fig. 8B), and 95kyr cycle (Fig. 8C), relative to their respective average thicknesses, reveal that the increase in accommodation mainly occurred during the PS-5 to PS-7 parasequences (95kyr cycles 5 to 7). This period of enhanced subsidence was both preceded and followed by periods characterized by reduced tectonic subsidence. These periods roughly correlate with, and could be responsible for, the three sets of parasequences (SPS-1, SPS-2 and SPS-3) and the three stages distinguished in the evolution of the lake system: LESL, MSCL and HEL.

Thus, LESL facies associations are characteristic of overfilled lake basins where the sedimentation rate exceeds the available accommodation (Alonso Zarza *et al.*, 2006; Carroll and Bohacs, 1999; Meléndez *et al.*, 2009). This scenario is consistent with the low subsidence expected during the initial rifting phase (Liesa *et al.*, 2006; Meléndez *et al.*, 2009). Subsequently, the lake system evolved into a mixed lake (MSCL) due to an increase in clastic supply and/or a decrease in carbonate production, associated with an increase in tectonic subsidence that marks the transition to the rifting climax (Liesa *et al.*, 2006). This phase was responsible for the abrupt deepening associated with SPS-2. The increased clastic supply could have been driven by a rejuvenation of relief caused by tectonic uplift during the rifting period. However, the influence of climatic factors cannot be ruled out, as increased humidity and runoff could also have led to an increase in surface water reaching the lake, thereby increasing clastic supply and causing further lake deepening. Furthermore, the supply of sulfate from groundwater into the lake might have altered the environmental conditions, disrupting carbonate production. Finally, as tectonic subsidence slowed, the clastic input to the basin decreased, and carbonate production resumed in a larger, more energetic carbonate lake. During this stage, typical lacustrine littoral facies characteristic of a balanced-fill lake basin developed, as suggested by the more complete lacustrine sequences identified in this phase (Meléndez *et al.*, 2009).

The results derived from the analysis of elementary sequence thicknesses are consistent with those observed in the parasequences and 95kyr cycles (Fig. 8B-C), further supporting the idea that tectonic forcing influenced subsidence changes across different time scales. However, the elementary sequences also exhibit a more pulsating variation, with thicker sequences (3.5-4.0m; *e.g.* ES-17, ES-19, ES-33, ES-35 or ES-36) alternating with thinner ones (1.5-2.0m; *e.g.* ES-15, ES-18, ES-34 or ES-37). This probably indicates that, over shorter time periods, tectonic subsidence occurred in a more discontinuous manner due to the pulsating activity of local normal faults. This could explain the periodicity of ~1.5m also identifed by

Illueca *et al.* (2023). It is plausible that this periodicity corresponds to the precession cycle during periods of lower sedimentation rates, rather than a half-precession cycle (~10kyr; Berger and Loutre, 1997; Boulila *et al.*, 2010; Park *et al.*, 1993) as proposed by Illueca *et al.* (2023). Similar instances of multiple periodicities linked to a single orbital cycle, associated with changes in fault activity, have been documented in other lacustrine synrift deposits (Casas *et al.*, 2024; Muñoz *et al.*, 2020; Soria *et al.*, 2012).

Examined in detail, the cumulative thickness deviation curve of elementary sequences reveals two periods of enhanced tectonic subsidence: a main period from ES-15 to ES-23 (PS-4 to PS-6) and an initial, shorter phase of accommodation creation during ES-4 and ES-5 (PS-1). Both phases were followed by periods of reduced accommodation creation (Fig. 8B). These findings suggest that the cycles of increasing and decreasing tectonics are asymmetric, with shorter durations for accelerating tectonic subsidence compared to longer periods of deceleration. Accelerated tectonic periods typically span two consecutive elementary sequences (40-50kyr), whereas decelerating tectonic periods are longer, usually exceeding 100kyr. Exceptions occur when several accelerating tectonic periods cluster to form a higher-order period, such as the one identified between ES-15 and ES-23. In such cases, brief periods of quiescence separate two periods of increasing tectonic activity. This pattern mirrors the slip history of faults observed in recent rift systems (*e.g.* Ezquerro *et al.*, 2015, 2016; Simón *et al.*, 2016).

Despite the significant influence of tectonics as the main factor generating accommodation and driving changes in the thicknesses of the sedimentary sequences and cycles across various time scales, the sedimentary and climatic cyclicity was not entirely obscured. This study has not accounted for other potential factors that might disrupt cyclicity, such as diagenetic processes (*i.e.* cementation, dissolution), sediment compaction, or variations in carbonate production and clastic supply during basin filling. Even though these processes can distort and complicate an assessment of astronomical influence (Meyers, 2019), they are interpreted as having less impact on the thickness and stacking patterns of lacustrine sequences compared to extensional tectonics. It is likely that their effects were more pronounced in smaller-scale sequences.

CONCLUSIONS

The nine lacustrine facies associations distinguished in the synrift El Castellar Formation mainly correspond to shallowing-upward sequences that developed in different subenvironments within a shallow lacustrine system. This system evolved through three stages over time: a low-energy shallow lake, a mixed siliciclastic-carbonate lake, and a high-energy lake. Three hierarchically stacked high-frequency lacustrine sequences are distinguished, resulting in the identification of 44 elementary sequences, ten complete parasequences (and two incomplete ones), and three sets of parasequences (one of them incomplete). The average thicknesses of these stratigraphic sequences are 2.9m (ranging from 1.25 to 5.25m), 12.4m (9.75 to 17.5m), and approximately 54m, respectively. The stratigraphic sequences are bounded by clear stratification surfaces that reflect flooding events following episodes of subaerial exposure. The elementary sequences, parasequences, and sets of parasequences align with the main periodicities of 3.3, 13.2 and 57m, corresponding respectively to the long precession cycle (22.4kyr) and to the short (95kyr) and long (405kyr) eccentricity cycles of the Earth's orbit. These correlations provide a robust linkage between the high-frequency lacustrine sequences and climate forcing driven by the Earth's orbital variations.

Variations in the thicknesses of elementary sequences and parasequences, as well as 95kyr cycles, are attributed to changes in accommodation related to tectonic activity associated with normal faults. An asymmetric cycle of >700kyr, characterized by alternating phases of increasing and decreasing tectonics, marks the transition from rift initiation to rifting climax stages, with an accelerated tectonic phase lasting around 200kyr. The changes in accommodation exhibit brief periods of increased tectonic subsidence lasting about 40-50kyr followed by longer (>100kyr) periods of decreased subsidence. The major phase of accelerated tectonics contributed to the deepening of the lake, an increased clastic supply, and the development of a mixed siliciclastic-carbonate lake system.

DECLARATION OF COMPETING INTEREST

The authors declare that they have no known competing financial interests or personal relationships that could have appeared to influence the work reported in this paper.

ACKNOWLEDGMENTS

The authors thank Marian Fregenal-Martínez, an anonymous reviewer, and editor Telm Bover-Arnal for their valuable comments and suggestions, and Rupert Glasgow for improving the English text. We would like to acknowledge the Servicio General de Apoyo a la Investigación-SAI from the Universidad de Zaragoza. This research has been financed by the Agencia Estatal de Investigación (MCIU/AEI/10.13039/501100011033) of the Spanish Government (grants PID2019-108705-GB-I00 and PID2023-148949NB-I00) and the Gobierno de Aragón (grant E32_23R of the GEOtransfer Research Group). N.I. benefits

from an INVESTIGO Program contract within the Recovery, Transformation and Resilience Plan, financed by the European Union-NextGenerationEU.

REFERENCES

Alonso-Zarza, A.M., Wright, V.P., 2010. Palustrine carbonates. In: Alonso-Zarza, A.M., Tanner, L.H. (eds.). Carbonates in Continental Settings: Geochemistry, Diagenesis and Applications. Developments in Sedimentology, 61, 103-132. DOI: https://doi.org/10.1016/S0070-4571(09)06102-0

Alonso-Zarza, A.M., Dorado-Valiño, M., Valdeolmillos-Rodríguez, A., Ruiz-Zapata, B., 2006. A recent analogue for palustrine carbonate environments: The Quaternary deposits of Las Tablas de Daimiel wetlands, Ciudad Real, Spain. Geological Society of America, 416 (Special Paper), 153-168. DOI: https://doi.org/10.1130/2006.2416(10)

Angulo, A., Muñoz, A., 2013. Análisis de la periodicidad climática de baja frecuencia registrada en los sedimentos lacustres del Grupo Enciso (Cretácico inferior de la Cuenca de Cameros, La Rioja). Aplicaciones a la correlación y datación de la serie. Boletín Geológico y Minero de España, 124(2), 203-219.

Anselmetti, F.S., Ariztegui, D., Hodell, D.A., Hillesheim, M.B., Brenner, M., Gilli, A., McKenzie, J.A., Mueller, A.D., 2006. Late Quaternary climate-induced lake level variations in Lake Petén Itzá, Guatemala, inferred from seismic stratigraphic analysis. Palaeogeography, Palaeoclimatology, Palaeoecology, 230(1-2), 52-69. DOI: https://doi.org/10.1016/j.palaeo.2005.06.037

Argylian, E.P., Forman, S.T., 2003. Lake level response to seasonal climatic variability in the Lake Michigan-Huron System from 1920 to 1995. Journal of Great Lakes Research, 29(3), 488-500. DOI: https://doi.org/10.1016/S0380-1330(03)70453-5

Armenteros, I., Huerta, P., 2006. The role of clastic sediment influx in the formation of calcrete and palustrine facies: a response to paleographic and climatic conditions in the southeastern Tertiary Duero basin (northern Spain). In: Alonso-Zarza, A.M., Tanner, L.H. (eds.). Paleoenvironmental Record and Applications of Calcretes and Palustrine Carbonates. Geological Society of America, 416 (Special Paper), 119-132. DOI: https://doi.org/10.1130/2006.2416(08)

Aurell, M., Bádenas, B., Gasca, J.M., Canudo, J.I., Liesa, C., Soria, A.R., Moreno-Azanza, M., Najes, L., 2016. Stratigraphy and evolution of the Galve sub-basin (Spain) in the middle Tithonian-early Barremian: implications for the setting and age of some dinosaur fossil sites. Cretaceous Research, 65, 138-162. DOI: https://doi.org/10.1016/j.cretres.2016.04.020

Azennoud, K., Baali, A., Mesquita-Joanes, F., El Asmi, H., Ait-Brahim, Y., 2023. Disentangling orbital, sub-orbital, and tectonic signatures from lacustrine sediments developed upon a half-graben (Lake Ifrah Basin, Northwest Africa): Insights into lowest-rank T-R sequences in low accommodation basins. Sedimentary Geology, 449, 106376. DOI: https://doi.org/10.1016/j.sedgeo.2023.106376

Aziz, H.A., Hilgen, F., Krijgsman, W., Sanz, E., Calvo, J.P., 2000. Astronomical forcing of sedimentary cycles in the middle to late Miocene continental Calatayud Basin (NE Spain). Earth and Planetary Science Letters, 177(1-2), 9-22. DOI: https://doi.org/10.1016/S0012-821X(00)00035-2

Barron, E.J., Washington, W.M., 1984. The role of geographic variables in explaining paleoclimates: Results from Cretaceous climate model sensitivity studies. Journal of Geophysical Research: Atmospheres, 89(D1), 1267-1279. DOI: https://doi.org/10.1029/JD089iDOIp01267

Berger, A., Loutre, M.F., McIntyre, A., 1997. Intertropical latitudes and precessional and half-precessional cycles/Response. Science, 278(5342), 1476-1478. Last accessed: 12 September 2024. Website: https://www.jstor.org/stable/2894768

Blakey, R., 2008. Gondwana palaeogeography from assembly to breakup – a 500m.y. odyssey. In: Fielding, C.R., Frank, T.D., Isbell, J.L. (eds.). Resolving the Late Paleozoic Ice Age in Time and Space. Geological Society of America, 441 (Special Paper), 1-28. DOI: https://doi.org/10.1130/2008.2441(01)

Bohacs, K.M., Carroll, A.R., Neal, J.E., Mankiewicz, P.J., 2000. Lake-basin type, source potential, and hydrocarbon character: an integrated sequence-stratigraphic geochemical framework. In: Gierlowski-Kordesch, E.H., Kelts, K.R. (eds.). Lake Basins through Space and Time. American Association of Petroleum Geologists Studies in Geology, 46, 3-33. DOI: https://doi.org/10.1306/St46706C1

Bosence, D.W.J., Procter E., Aurell, M., Bel Kahla, A., Boudagher-Fadel, M., Casaglia, F., Cirilli, S., Mehdie, M., Nieto, L., Rey, J., Scherreiks, R., Soussi, M., Waltham, D., 2009. A tectonic signal in high-frequency, peritidal carbonate cycles? A regional analysis of Liassic platforms from western Tethys. Journal of Sedimentary Research, 79, 389-415. DOI: https://doi.org/10.2110/jsr.2009.038

Boulila, S., Galburn, B., Hinnov, L.A., Collin, P.Y., Ogg, J.G., Fortwengler, D., Marchand, D., 2010. Milankovitch and sub□ Milankovitch forcing of the Oxfordian (Late Jurassic) Terres Noires Formation (SE France) and global implications. Basin Research, 22, 717-732. DOI: https://doi.org/10.1111/j.1365-2117.2009.00429.x

Boulila, S., Galbrun, B., Miller, K.G., Pekar, S.F., Browning, J.V., Laskar, J., Wright, J.D., 2011. On the origin of Cenozoic and Mesozoic "third-order" eustatic sequences. Earth-Science Reviews, 109, 94-112. DOI: https://doi.org/10.1016/j.earscirev.2011.09.003

Burgener, L., Hyland, E., Reich, B.J., Scotese, C., 2023. Cretaceous climates: Mapping plaeo-Köppen climatic zones using a Bayesian statistical analysis of lithologic, paleontologic, and geochemical proxies. Palaeogeography, Palaeoclimatology, Palaeoecology, 613, 11373. DOI: https://doi.org/10.1016/j.palaeo.2022.111373

Buscalioni, A.D., Fregenal Martínez, M.A., 2010. A holistic approach to the palaeoecology of Las Hoyas Konservat-Lagerstätte (La Huérguina Formation, Lower Cretaceous, Iberian Ranges, Spain). Journal of Iberian Geology, 36(2), 297-326. DOI: 10.5209/rev_JIGE.2010.v36.n2.13

Camuera, J., Jiménez-Moreno, G., Ramos-Román, M.J., García-Alix, A., Toney, J.L., Anderson, R.S., Jiménez-Espejo, F., Kaufman, D., Bright, J., Webster, C., Yanes, Y., Carrión, J.S., Ohkouchi, N., Suga, H., Yamame, M., Yokoyama, Y., Martínez-Ruiz, F., 2018. Orbital-scale environmental and climatic changes recorded in a new□200,000-year-long multiproxy sedimentary record from Padul, southern Iberian Peninsula. Quaternary Science Reviews, 198, 91-114. DOI: https://doi.org/10.1016/j.quascirev.2018.08.014

Capote, R., Muñoz, J.A., Simón, J.L., Liesa, C.L., Arlegui, L.E., 2002. Alpine Tectonics I: The Alpine System North of the Betic Cordillera. In: Gibbons, W., Moreno, T. (eds.). The Geology of Spain. London, The Geological Society, 367-400.

Carroll, A.R., Bohacs, K.M., 1999. Stratigraphic classification of ancient lakes: Balancing tectonic and climatic controls. Geology, 27(2), 99-102. DOI: https://doi.org/10.1130/0091-7613(1999)027<0099:SCOALB>2.3.CO;2

Casas, A.M., Muñoz, A., Tella, A., Liesa, C.L., 2024. Magnetic surveying as a proxy for defining cyclicity in thick sedimentary fillings: Application to the Cretaceous Cameros Basin (N Spain). Cretaceous Research, 154, 105736. DOI: https://doi.org/10.1016/j.cretres.2023.105736

Castanera, D., Bádenas, B., Aurell, M., Canudo, J.I., Gasca, J.M., 2022. New ornithopod tracks from the Lower Cretaceous El Castellar Formation (Spain): Implications for track preservation and evolution of ornithopod footprints. Palaeogeography, Palaeoclimatology, Palaeoecology, 591, 110866. DOI: https://doi.org/10.1016/j.palaeo.2022.110866

Catuneanu, O., 2022. Principles of sequence stratigraphy. Elsevier Science, 2nd Edition, 486pp. DOI: https://doi.org/10.1016/C2009-0-19363-5

Changsong, L., Eriksson, K., Sitian, L., Yongxian, W., Jianye, R., Yanmei, Z., 2001. Sequence architecture, depositional systems, and controls on development of lacustrine basin fills in part of the Erlian Basin, northeast China. American Association of Petroleum Geologists Bulletin, 85, 2017-2043. DOI: https://doi.org/10.1306/8626D0DB-173B-11D7-8645000102C1865D

Christie-Blick, N., 1991. Onlap, offlap, and the origin of unconformity-bounded depositional sequences. Marine Geology, 97, 35-56. DOI: https://doi.org/10.1016/0025-3227(91)90018-Y

Coianiz, L., Bialik, O.M., Ben-Avraham, Z., Lazar, M., 2019. Late Quaternary lacustrine deposits of the Dead Sea basin: high resolution sequence stratigraphy from downhole logging data. Quaternary Science Reviews, 210, 175-189. DOI: https://doi.org/10.1016/j.quascirev.2019.03.009

de Wet, C.B., Godfrey, L., de Wet, A.P., 2015. Sedimentology and stable isotopes from a lacustrine-to-palustrine limestone deposited in an arid setting, climatic and tectonic factors: Miocene–Pliocene Opache Formation, Atacama Desert, Chile. Palaeogeography, Palaeoclimatology, Palaeoecology, 426, 46-67. DOI: https://doi.org/10.1016/j.palaeo.2015.02.039

Deino, A.L., Kingston, J.D., Glen, J.M., Edgar, R.K., Hill, A., 2006. Precessional forcing of lacustrine sedimentation in the late Cenozoic Chemeron Basin, Central Kenya Rift, and calibration of the Gauss/Matuyama boundary. Earth and Planetary Science Letters, 247(1-2), 41-60. DOI: https://doi.org/10.1016/j.epsl.2006.04.009

Dercourt, J., Zonensshain, L.P., Ricou, L.E., Kazmin, V.G., Le Pichon, X., Knipper, A.L., Grandjacquet, C., Sbortshikov, I.M., Geyssant, J., Leprevier, C., Pechersky, D.H., Boulin, J., Sibuet, J.C., Savostin, L.A., Sorokhtin, O., Westphal, M., Bazhenov, M.L., Lauer, J.P., Biju-Duval, B., 1986. Geological evolution of the Tethys belt from the Atlantic to the Pamir since the Lias. Tectonophysics, 123, 241-315. DOI: https://doi.org/10.1016/0040-1951(86)90199-X

Emery, D., Myers, K. (eds.), 2009. Sequence stratigraphy. New Jersey, John Wiley & Sons, 309pp.

Ezquerro, L., 2017. El sector norte de la cuenca neógena de Teruel: tectónica, clima y sedimentación. PhD Thesis. Zaragoza, Universidad de Zaragoza, 494pp. Last accessed: 21 October 2024. Website: http://zaguan.unizar.es/record/77098#

Ezquerro, L., Moretti, M., Liesa, C.L., Luzón, A., Simón, J.L., 2015. Seismites from a well core of palustrine deposits as a tool for reconstructing the palaeoseismic history of a fault. Tectonophysics, 655, 191-205. DOI: http://dx.doi.org/10.1016/j.tecto.2015.05.025

Ezquerro, L., Moretti, M., Liesa, C.L., Luzón, A., Pueyo, E.L., Simón, J.L., 2016. Controls on space–time distribution of soft-sediment deformation structures: Applying palaeomagnetic dating to approach the apparent recurrence period of paleoseisms at the Concud Fault (eastern Spain). Sedimentary Geology, 344, 91-111. DOI: http://dx.doi.org/10.1016/j.sedgeo.2016.06.007

Ezquerro, L., Simón, J.L., Luzón, A., Liesa, C.L., 2020. Segmentation and increasing activity in the Neogene-Quaternary Teruel Basin rift (Spain) revealed by morphotectonic approach. Journal of Structural Geology, 135, 104043. DOI: https://doi.org/10.1016/j.jsg.2020.104043

Ezquerro, L., Muñoz, A., Liesa, C.L., Simón, J.L., Luzón, A., 2022a. Late Neogene to early Quaternary climate evolution in southwestern Europe from a continental perspective. Global and Planetary Change, 211, 103788. DOI: https://doi.org/10.1016/j.gloplacha.2022.103788Ezquerro, L., Luzón, A., Simón, J.L., Liesa, C.L., 2022b. A review of the European Neogene Mammal zones from integration of litho-, bio- and magnetostratigraphy in the Teruel Basin. Earth-Science Reviews, 234, 104223. DOI: https://doi.org/10.1016/j.earscirev.2022.104223

Fölmi, K.B., 2012. Early Cretaceous life, climate and anoxia. Cretaceous Research, 35, 230-257. DOI: https://doi.org/10.1016/j.cretres.2011.12.005

Fregenal-Martínez, M.A., Meléndez, N., 2000. The lacustrine fossiliferous deposits of the Las Hoyas Subbasin (Lower Cretaceous, Serranía de Cuenca, Iberian Ranges, Spain). In: Gierlowski-Kordesch, E.H., Kelts, K.R. (eds.). Lake Basins through Space and Time. American Association of Petroleum Geologists Studies in Geology, 46, 303-313. DOI: https://doi.org/10.1306/St46706C25

Friedmann, S.J., Burbank, D.W., 1995. Rift Basins and supradetachment basins: intracontinental extensional end-members. Basin Research, 7(2), 109-127. DOI: https://doi.org/10.1111/j.1365-2117.1995.tb00099.x

García-Penas, A., Aurell, M., 2017. Tectono-sedimentary evolution around the Jurassic-Cretaaceous transition in Galve (Aguilar del Alfambra Formation, Teruel, Iberian Chain). Revista de la Sociedad Geológica de España, 30(2), 79-90.

Gasca, J.M., Moreno-Azanza, M., Canudo, J.I., 2009. The dinosaur assemblage of the El Castellar Formation (upper Hauterivian-lowemost Barremian, Teruel, Spain). In: Godefroit, P., Lambert, O. (eds.). Tribute to Charles Darwin to Bernissart Iguanodons: New perspectives on Vertebrate Evolution and Early Cretaceous Ecosystems. Brussels (Belgium), Programme, Abstracts and Field Trips Guidebook, 43pp.

Gierlowski-Kordesch, E.H., Gómez-Fernández, J.C., Meléndez, N., 1991. Carbonate and coal deposition in an alluvial–lacustrine setting: Lower Cretaceous (Weald) in the Iberian Range (east–central Spain). In: Anadón, P., Cabrera, Ll., Kelts, K.R. (eds.). Lacustrine Facies Analysis. International Association of Sedimentologists, 13 (Special Publication), 109-125. DOI: https://doi.org/10.1002/9781444303919.ch6

Gomes, J.P.B., Bunevich, R.B., Tonietto, S.N., Alves, D.B., Santos, J.F., Whitaker, F.F., 2020. Climatic signals in lacustrine deposits of the Upper Yacoraite Formation, Western Argentina: evidence from clay minerals, analcime, dolomite and fibrous calcite. Sedimentology, 67(5), 2282-2309. DOI: https://doi.org/10.1111/sed.12700

Gómez-Fernández, J.C., Meléndez, N., 1994. Climatic control on Lower Cretaceous sedimentation in a playa–lake system of a tectonically active basin, Huérteles alloformation, Cameros Basin, (north–central Spain). Journal of Paleolimnology, 11, 91-107. DOI: https://doi.org/10.1007/BF00683272

Gong, Z., Langereis, C.G., Mullender, T.A.T., 2008. The rotation of Iberia during the Aptian and the opening of the Bay of Biscay. Earth and Planetary Science Letters, 273, 80-93. DOI: https://doi.org/10.1016/j.epsl.2008.06.016

Guiter, F., Andrieu-Ponel, V., de Beaulieu, J.L., Cheddadi, R., Calvez, M., Ponel, P., Reille, M., Keller, T., Goeury, C., 2003. The last climatic cycles in Western Europe: a comparison between long continuous lacustrine sequences from France and other terrestrial records. Quaternary International, 111(1), 59-74. DOI: https://doi.org/10.1016/S1040-6182(03)00015-6

Hammer, Ø., Harper, D.A.T., Ryan, P.D., 2001. PAST: Paleontological statistics software package for education and data analysis. Paleontologia Electronica, 4(1), 1-9. Last accessed: 21 October 2024. Website: http://palaeoelectronica.org

Hasegawa H., Katsuta, N., Muraki, Y., Heimhofer, U., Ichinnorov, N., Asahi, H., Ando, H., Yamamoto, K., Murayama, M., Ohta, T., Yamamoto, M., Ikeda, M., Ishikawa, K., Kuma, R., Hasegawa, T., Hasebe, N., Nishimoto, S., Yamaguchi, K., Abe, F., Tada, R., Nakagawa, T., 2022. Decadal–centennial-scale solar-linked climate variations and millennial-scale internal oscillations during the Early Cretaceous. Scientific Reports, 12, 21894. DOI: https://doi.org/10.1038/s41598-022-25815-w

Hay, W.W., Floegel, S., 2012. New thoughts about the Cretaceous climate and oceans. Earth-Science Reviews, 115(4), 262-272. DOI: https://doi.org/10.1016/j.earscirev.2012.09.008

Haywood, A.M., Valdes, P.J., Markwick, P.J., 2004. Cretaceous (Wealden) climates: a modelling perspective. Cretaceous Research, 25(3), 303-311. DOI: https://doi.org/10.1016/j.cretres.2004.01.005

Hoorn, C., Kukla, T., Bogotá□Angel, G., van Soelen, E., González□Arango, C., Wesselingh, F.P., Vonhof, H., Val, P., Morcote□Rios, G., Roddaz, M., Luiz Dantas, E., Ventura Santos, R., Sinninghe Damsté, J.S., Kim, J.-H., Morley, R.J., 2022. Cyclic sediment deposition by orbital forcing in the Miocene wetland of western Amazonia? New insights from a multidisciplinary approach. Global and Planetary Change, 210, 103717. DOI: https://doi.org/10.1016/j.gloplacha.2021.103717

Huang, C., Ogg, J.G., Kemp, D.B., 2020. Cyclostratigraphy and astrochronology: Case studies from China. Palaeogeography, Palaeoclimatology, Palaeoecology, 560, 110017. DOI: https://doi.org/10.1016/j.palaeo.2020.110017

Ielpi, A., 2012. Orbitally-driven climate forcing in late Pliocene lacustrine siderite-rich clastic rhythms (Upper Valdarno Basin, Northern Apennines, Italy). Palaeogeography, Palaeoclimatology, Palaeoecology, 331, 119-135. DOI: https://doi.org/10.1016/j.palaeo.2012.03.004

Illueca, N., Liesa, C.L., Soria, A.R., 2023. Ciclicidad climática en sedimentos lacustres de la Formación El Castellar (Cretácico inferior, Cordillera Ibérica). Geogaceta, 74, 3-6. DOI: https://doi.org/10.55407/geogaceta98398

Jervey, M.T., 1988. Quantitative geological modelling of siliciclastic rock sequences and their seismic expression. In: Wilgus, C.K., Hastings, B.S., Kendall, C.G.St.C., Posamentier, H.W., Ross, C.A., Van Wagoner, J.C. (eds.). Sea Level Changes – An Integrated Approach. Society of Economic Paleontologists and Mineralogists (SEPM), 42 (Special Publication), 47-69. DOI: https://doi.org/10.2110/pec.88.01.0047

Jin, Z., Yu, J., Zhang, F., Qiang, X., 2020. Glacial-interglacial variation in catchment weathering and erosion paces the Indian summer monsoon during the Pleistocene. Quaternary Science Reviews, 248, 106619. DOI: https://doi.org/10.1016/j.quascirev.2020.106619

Juhász, E., Kovács, L.Ó., Müller, P., Tóth-Makk, A., Phillips, L., Lantos, M., 1997. Climatically driven sedimentary cycles in the Late Miocene sediments of the Pannonian Basin, Hungary. Tectonophysics, 282(1-4), 257-276. DOI: https://doi.org/10.1016/S0040-1951(97)00222-9

Keighley, D., Flint, S., Howell, J., Moscariello, A., 2003. Sequence stratigraphy in lacustrine basins: A model for part of the Green River Formation (Eocene), Southwest Uinta Basin, Utah, U.S.A. Journal of Sedimentary Research, 73(6), 987-1006. DOI: https://doi.org/10.1306/050103730987

King, M.T., Welford, J.K., Cadenas, P., Tugend, J., 2021. Investigating the plate kinematics of the Bay of Biscay using deformable plate tectonic models. Tectonics, 40, e2020TC006467. DOI: https://doi.org/10.1029/2020TC006467

Kovács, Á., Balázs, A., Špelić, M., Sztanó, O., 2021. Forced or normal regression signals in a lacustrine basin? Insights from 3D stratigraphic forward modeling in the SW Pannonian Basin. Global and Planetary Change, 196, 103376. DOI: https://doi.org/10.1016/j.gloplacha.2020.103376

Kuzucuoğlu, C., Karabiyikoğlu, M., Fontugne, M., Pastre, J.F., Ercan, T., 1997. Environmental changes in Holocene lacustrine sequences from Karapinar in the Konya plain (Turkey). In: Dalfes, H.N., Kukla, G., Weiss, H. (eds.). Third Millennium BC Climate Change and Old World Collapse. Berlin, Heidelberg, Springer, NATO ASI Series, 49, 451-463. DOI: https://doi.org/10.1007/978-3-642-60616-8_18

Laita, E., Bauluz, B., Aurell, M., Bádenas, B., Canudo, J.I., Yuste, A., 2020. A change from warm/humid to cold/dry climate conditions recorded in lower Barremian clay-dominated continental successions from the SE Iberian Chain (NE Spain). Sedimentary Geology, 403, 105673. DOI: https://doi.org/10.1016/j.sedgeo.2020.105673

Laita, E., Bauluz, B., Aurell, M., Bádenas, B., Yuste, A., 2022. Weathering events recorded in uppermost Hauterivian–lower Barremian clay-dominated continental successions from the NW Iberian Range: climatic vs. tectonic controls. Journal of Iberian Geology, 48, 45-63. DOI: https://doi.org/10.1007/s41513-021-00181-0

Leeder, M.R., 1991. Denudation, vertical crustal movements and sedimentary basin fill. Geologische Rundschau, 80, 441-458. DOI: 10.1007/bf01829376

Lepre, C.J., Quinn, R.L., 2022. Aridification and orbital forcing of eastern African climate during the Plio-Pleistocene. Global and Planetary Change, 208, 103684. DOI: https://doi.org/10.1016/j.gloplacha.2021.103684

Li, M., Kump, L.R., Hinnov, L.A., Mann, M.E., 2018. Tracking variable sedimentation rates and astronomical forcing in Phanerozoic paleoclimate proxy series with evolutionary correlation coefficients and hypothesis testing. Earth and Planetary Science Letters, 501, 165-179. DOI: https://doi.org/10.1016/j.epsl.2018.08.041

Liesa, C.L., Casas, A.M., Soria, A.R., Simón, J.L., Meléndez, A., 2004. Estructura extensional cretácica e inversión terciaria en la región Aliaga-Montalbán. In: Colombo, F., Liesa, C.L., Meléndez, G., Pocoví, A., Sancho C., Soria, A.R. (eds.). Itinerarios Geológicos por Aragón. Zaragoza, Sociedad Geológica de España, 151-180.

Liesa, C.L., Soria, A.R., Meléndez, N., Meléndez, A., 2006. Extensional fault control on the sedimentation patterns in a continental rift basin: El Castellar Formation, Galve subbasin, Spain. Journal of the Geological Society, 163(3), 487-498. DOI: https://doi.org/10.1144/0016-764904-169

Liesa, C.L., Casas, A.M., Simón, J.L., 2018. La tectónica de inversión en una región intraplaca: la Cordillera Ibérica. Revista de la Sociedad Geológica de España, 31(2), 23-50.

Liesa, C.L., Soria, A.R., Casas, A., Aurell, M., Meléndez, N., Bádenas, B., Fregenal-Martínez, M., Navarrete, R., Peropadre, C., Rodríguez-López, J.P., 2019. The South-Iberian, Central Iberian and Maestrazgo Basins. In: Oliveira, J.T., Quesada, C. (eds.). The Geology of Iberia: a Geodynamic Approach, Vol. 3 (The Alpine Cycle), (Chapter 5) (Late Jurassic-Early Cretaceous rifting). Springer Nature, Regional Geology Reviews, 214-228. DOI: https://doi.org/10.1007/978-3-030-11295-0_5

Liesa, C.L., Casas, A.M., Aurell, M., Simón, J.L., Soria, A.R., 2023. Salt tectonics vs. inversion tectonics: The anticlines of the western Maestrazgo revisited (eastern Iberian Chain, Spain). Basin Research, 35, 295-335. DOI: https://doi.org/10.1111/bre.12713

Luzón, A., González, A., Muñoz, A., Sánchez-Valverde, B., 2002. Upper Oligocene-Lower Miocene shallowing-upward lacustrine sequences controlled by periodic and non-periodic processes (Ebro Basin, northeastern Spain). Journal of Paleolimnology, 28, 441-456. DOI: https://doi.org/10.1023/A:1021675227754

Martín-Chivelet, J., López-Gómez, J., Aguado, R., Arias, C., Arribas, J., Arribas, M.E., Aurell, M., Bádenas, B., Benito, M.I., Bover-Arnal, T., Casas-Sainz, A., Castro, J.M., Coruña, F., de Gea, G.A., Fornós, J.J., Fregenal-Martínez, M., García-Senz, J., Garófano, D., Gelabert, B., Giménez, J., González-Acebrón, J., Guimerà, J., Liesa, C.L., Mas, R., Meléndez, N., Molina, J.M., Muñoz, J.A., Navarrete, R., Nebot, M., Nieto, L.M., Omodeo-Salé, S., Pedrera, A., Peropadre, C., Quijada, I.E., Quijano, M.L., Reolid, M., Robador, A., Rodríguez-López, J.P., Rodríguez-Perea, A., Rosales, I., Ruiz-Ortiz, P.A., Sàbat, F. Salas, R., Soria, A.R., Suárez-González, P., Vilas, L., 2019. The Late Jurassic-Early Cretaceous Rifting. In: Quesada, C., Oliveira, J.T. (eds.). The Geology of Iberia: A Geodynamic Approach, The Alpine Cycle. Springer Nature, Regional Geology Reviews, vol. 5, 169-249. DOI: https://doi.org/10.1007/978-3-030-11295-0_5

Meléndez, M.N., Liesa, C.L., Soria, A.R., Meléndez, A., 2009. Lacustrine system evolution during early rifting: El Castellar Formation (Galve sub-basin, Central Iberian Chain). Sedimentary Geology, 222, 64-77. DOI: https://doi.org/10.1016/j.sedgeo.2009.05.019

Meléndez, M.N., Soria, A.R., Meléndez, A., Aurell, M., Liesa, C.L., 2000. Early Cretaceous lacustrine systems of the Aguilón Subbasin (Central Iberian range, NE Spain): tectonic evolution. In: Gierlowski-Kordesch, E.H., Kelts, K.R. (eds.). Lake Basins through Space and Time. American Association of Petroleum Geologists Studies in Geology, 46, 285-294. DOI: https://doi.org/10.1306/St46706C23

Meyers, S.R., 2019. Cyclostratigraphy and the problem of astrochronologic testing. Earth-Science Reviews, 190, 190-223. DOI: https://doi.org/10.1016/j.earscirev.2018.11.015

Milankovitch, M.M., 1941. Canon of insolation and the iceage problem. Koniglich Serbische Akademice, 484pp.

Ming, G., Zhou, W., Wang, H., Cheng, P., Shu, P., Xian, F., Fu, Y., 2020. Moisture variations in Lacustrine–eolian sequence from the Hunshandake sandy land associated with the East Asian Summer Monsoon changes since the late Pleistocene. Quaternary Science Reviews, 233, 106210. DOI: https://doi.org/10.1016/j.quascirev.2020.106210

Mitchum, R.M., Van Wagoner, J.C., 1991. High-frequency sequences and their stacking patterns: sequence-stratigraphic evidence of high-frequency eustatic cycles. Sedimentary Geology, 70, 131-160. DOI: https://doi.org/10.1016/0037-0738(91)90139-5

Moreau, M.G., Berthou, J.Y., Malod, J.A., 1997. New paleomagnetic Mesozoic data from the Algarve (Portugal): fast rotation of Iberia between the Hauterivian and the Aptian. Earth and Planetary Science Letters, 146, 689-701. DOI: https://doi.org/10.1016/S0012-821X(96)00239-7

Moreno, A., González-Sampériz, P., Morellón, M., Valero-Garcés, B.L., Fletcher, W.J., 2012. Northern Iberian abrupt climate change dynamics during the last glacial cycle: a view from lacustrine sediments. Quaternary Science Reviews, 36, 139-153. DOI: https://doi.org/10.1016/j.quascirev.2010.06.031

Moriya, K., 2011. Development of the Cretaceous greenhouse climate and the oceanic thermal structure. Paleontological Research, 15(2), 77-88. DOI: https://doi.org/10.2517/1342-8144-15.2.077

Morrill, C., Small, E.E., Sloan, L.C., 2001. Modeling orbital forcing of lake level change: Lake Gostiute (Eocene), North America. Global and Planetary Change, 29, 57-76. DOI: https://doi.org/10.1016/S0921-8181(00)00084-9

Muñoz, A., Angulo, A., Liesa, C.L., Luzón, M.A., Mayayo, M.J., Pérez, A., Soria, A.R., Val, V., Yuste, A., 2020. Climatic periodicities and astrochronological dating of the Enciso Group in the eastern Cameros Basin (N of Spain). Boletín Geológico y Minero, 131(2), 243-268. DOI: https://doi.org/10.21701/bolgeomin.131.2.003

Murphy, D.H. Wilkinson, B.H., 1980. Carbonate deposition and facies distribution in a central Michigan marl lake. Sedimentology, 27, 123-135. DOI: https://doi.org/10.1111/j.1365-3091.1980.tb01164.x

Navarrete, R., 2015. Controles alocíclicos de la sedimentación barremiense en la Subcuenca de Galve (Fm. Camarillas, margen occidental de la Cuenca del Maestrazgo). PhD Thesis. Zaragoza, Universidad de Zaragoza, 448pp.

Nutz, A., Schuster, M., Boës, X., Rubino, J.L., 2017. Orbitally-driven evolution of Lake Turkana (Turkana Depression, Kenya, EARS) between 1.95 and 1.72 Ma: A sequence stratigraphy perspective. Journal of African Earth Sciences, 125, 230-243. DOI: https://doi.org/10.1016/j.jafrearsci.2016.10.016

O'Connor, L., Robinson, S.A., Naafs, B.D.A., Jenkyns, H.C., Henson, S., Clarke, M., Pancost, R.D., 2019. Late Cretaceous temperature evolution of the southern high latitudes: A TEX86 perspective. Paleoceanography and Paleoclimatology, 34, 436-454. DOI: https://doi.org/10.1029/2018PA003546

Oviatt, Ch., Mccoy, W.D., Nash, W.P., 1994. Sequence stratigraphy of lacustrine deposits: A Quaternary example from the Bonneville basin, Utah. Geological Society of America Bulletin, 106(1), 133-144. DOI: https://doi.org/10.1130/0016-7606(1994)106<0133:SSOLDA>2.3.CO;2

Park, J., d'Hont, S.L., King, J.W., Gibson, C., 1993. Late Cretaceous precessional cycles in double time: A warm-Earth Milankovitch response. Science, 261(5127), 1431-1434. DOI: 10.1126/science.261.5127.1431

Platt, N.H., Wright, V.P., 1991. Lacustrine carbonates: facies models, facies distribution and hydrocarbon aspects. In: Anadón, P., Cabrera, L., Kelts, K. (eds.). Lacustrine Facies Analysis. Special Publication International Association of Sedimentologists, 13, 57-74.

Platt, N.H., Wright, V.P., 1992. Palustrine carbonates and the Florida Everglades: towards and exposure index for the fresh-water environment? Journal Sedimentary Petrology, 62, 1058-1071. DOI: https://doi.org/10.1306/D4267A4B-2B26-11D7-8648000102C1865D

Posamentier, H.W., Vail, P.R., 1988. Eustatic controls on clastic deposition II: Sequence and systems tract models. In: Wilgus, C.K., Hastings, B.S., Posamentier, H., Van Wagoner, J., Ross, C.A., Kendall, C.G.St.C. (eds.). Sea Level Changes: An Integrated Approach. Society of Economic Paleontologists and Mineralogists (SEPM), 42 (Special Publication), 125-154. DOI: https://doi.org/10.2110/pec.88.01.0125

Rits, D.S., van Balen, R.T., Prins, M.A., Zheng, H., 2017. Evolution of the alluvial fans of the Luo River in the Weihe Basin, central China, controlled by faulting and climate change-A reevaluation of the paleogeographical setting of Dali Man site. Quaternary Science Reviews, 166, 339-351. DOI: https://doi.org/10.1016/j.quascirev.2017.01.013

Rodríguez-López, J.P., Wu, C., Vishnivetskaya, T.A., Murton, J.B., Tang, W., Ma, C., 2022. Permafrost in the Cretaceous supergreenhouse. Nature Communications, 13, 7946. DOI: https://doi.org/10.1038/s41467-022-35676-6

Rodríguez-López, J.P., Liesa, C.L., Luzón, A., Muñoz, A., Mayayo, M.J., Murton, J.B., Soria, A.R., 2024. Ice-rafted dropstones at midlatudes in the Cretaceous of continental Iberia. Geology, 52, 33-38. DOI: https://doi.org/10.1130/G51725.1

Rosenbaum, G., Lister, G.S., Duboz, C., 2002. Relative motions of Africa, Iberia and Europe during Alpine orogeny. Tectonophysics, 359, 117-129. DOI: https://doi.org/10.1016/S0040-1951(02)00442-0

Ruddiman, W.F., 2006. Orbital changes and climate. Quaternary Science Reviews, 25, 3092-3112. DOI: https://doi.org/10.1016/j.quascirev.2006.09.001

Ruiz Omeñaca, J.I., 2006. Restos directos de dinosaurios (Saurischia, Ornithischia) en el Barremiense (Cretácico Inferior) de la Cordillera Ibérica en Aragón (Teruel, España). PhD Thesis. Zaragoza, Universidad de Zaragoza, 432pp.

Sáez, A., Valero-Garces, B.L., Giralt, S., Moreno, A., Bao, R., Pueyo, J.J., Hernández, A., Casas, D., 2009. Glacial to Holocene climate changes in the SE Pacific. The Raraku lake sedimentary record (Easter Island, 27 S). Quaternary Science Reviews, 28(25-26), 2743-2759. DOI: https://doi.org/10.1016/j.quascirev.2009.06.018

Salas, R., 1987. El Malm i el Cretaci inferior entre el Massís de Garraf i la Serra d'Espadà: anàlisi de conca. PhD Thesis. Barcelona, Universitat de Barcelona, 345pp.

Salas, R., Casas, A., 1993. Mesozoic extensional tectonics, stratigraphy and crustal evolution during the Alpine cycle of

the eastern Iberian basin. Tectonophysics, 228, 33-55. DOI: https://doi.org/10.1016/0040-1951(93)90213-4

Salas, R., Guimerà, J., Mas, R., Martín-Closas, C., Meléndez, A., Alonso, A., 2001. Evolution of the Mesozoic central Iberian Rift System and its Cainozoic inversion (Iberian Chain). In: Ziegler, P.A., Cavazza, W., Robertson, A.H.F., Crasquin-Soleau, S. (eds.). Peri-Tethyan Rift/Wrench Basins and Passive Margins. Peri-Tethys Memoir 6: Peri-Tethyan Rift/Wrench Basins and Passive Margins. Paris, Muséum national d'Histoire naturelle, 186, 145-185.

Sames, B., Wagreich, M., Wendler, J.E., Haq, B.U., Conrad, C.P., Melinte-Dobrinescu, M.C., Hu, X., Wendler, I., Wolfgring, E., Yilmaz, I.Ö, Zorina, S.O., 2016. Review: Short-term seal-level changes in a greenhouse world – A review from the Cretaceous. Palaeogeography, Palaeoclimatology, Palaeoecology, 441, 393-411. DOI: https://doi.org/10.1016/j.palaeo.2015.10.045

Scheidt, S., Hambach, U., Hao, Q., Rolf, C., Wennrich, V., 2020. Environmental signals of Pliocene-Pleistocene climatic changes in Central Europe: Insights from the mineral magnetic record of the Heidelberg Basin sedimentary infill (Germany). Global and Planetary Change, 187, 103112. DOI: https://doi.org/10.1016/j.gloplacha.2020.103112

Schnyder, J., Dejax, J., Keppens, E., Tu, T.T.N., Spagna, P., Boulila, S., Galbrun, B., Riboulleau, A., Tshibangu, J.P., Yans, J., 2009. An Early Cretaceous lacustrine record: organic matter and organic carbon isotopes at Bernissart (Mons Basin, Belgium). Palaeogeography, Palaeoclimatology, Palaeoecology, 281(1-2), 79-91. DOI: https://doi.org/10.1016/j.palaeo.2009.07.014

Schwarzacher, W., 2005. The stratification and cyclicity of the Dachstein Limestone in Lofer, Leogang and Steinernes Meer (Northern Calcareous Alps, Austria). Sedimentary Geology, 181, 93-106. DOI: https://doi.org/10.1016/j.sedgeo.2005.07.001

Scotese, C.R., 2016. Tutorial: PALEOMAP Paleoatlas for GPlates and the PaleoData Plotter Program. Tutor, PALEOMAP Project. Last accessed: 12 September 2024. Website: http://www.earthbyte.org/paleomap-paleoatlas-for-gplates/

Sevillano, A., Bádenas, B., Rosales, I., Barnolas, A., López-García, J.M., 2020. Orbital cycles, differential subsidence and internal factors controlling the high-frequency sequence architecture in a Sinemurian shallow carbonate platform (Mallorca Island, Spain). Sedimentary Geology, 407, 105729. DOI: https://doi.org/10.1016/j.sedgeo.2020.105729.

Simmons, G.F., 2016. Differential Equations with Applications and Historical Notes. Boca Raton, CRC Press, 740pp.

Simón, J.L., Arlegui1, L.E., Ezquerro, L., Lafuente, P., Liesa, C.L., Luzón, A., 2016. Enhanced palaeoseismic succession at the Concud Fault (Iberian Chain, Spain): new insights for seismic hazardassessment. Natural Hazards, 80, 1967-1993. DOI: https://doi.org/10.1007/s11069-015-2054-6

Soria, A.R., 1997. Estudio estratigráfico-sedimentológico y tectónico del Cretácico inferior en la parte occidental de la cuenca del Maestrazgo, subcuencas de Las Parras y Galve. La sedimentación en las cuencas marginales del surco ibérico durante el Cretácico Inferior y su control estructural. PhD Thesis. Zaragoza, Universidad de Zaragoza, 363pp.

Soria, A.R., Liesa, C.L., Meléndez, A., Meléndez, M.N., 2001. Sedimentación sintectónica de la Fm. El Castellar (Cretácico Inferior) en la Subcuenca de Galve (Cuenca Ibérica). Geotemas, 3, 257-260.

Soria, A.R., Muñoz, A., Liesa, C.L., Meléndez, A., Meléndez, M.N., Soto, R., 2008. Ciclicidad climática en una unidad lacustre cretácica: la Fm. Villanueva de Huerva en la Subcuenca de Aguilón (Cordillera Ibérica). Geotemas, 10, 1487-1490.

Soria, A.R., Muñoz, A., Liesa, C.L., Luzón, A., Meléndez, A., Meléndez, M.N., 2012. Climate-driven cyclicity in an Early Cretaceous synrift lacustrine series (Aguilón subbasin, NE Spain). Terra Nova, 24, 407-416. DOI: https://doi.org/10.1111/j.1365-3121.2012.01080.x

Soria, A.R., Liesa, C.L., Navarrete, R., Rodríguez-López, J.P., 2023. Sedimentology and stratigraphic architecture of Barremian synrift barrier island–estuarine depositional systems from blended field and drone-derived data. Sedimentology, 70, 1812-1855. DOI: https://doi.org/10.1111/sed.13097.

Stampfli, G.M., Borel, G.D., 2002. A plate tectonic model for the Paleozoic and Mesozoic constrained by dynamic plate boundaries and restored synthetic oceanic isochrons. Earth and Planetary Science Letters, 196, 17-33. DOI: https://doi.org/10.1016/S0012-821X(01)00588-X

Steenbrink, J., Hilgen, F.J., Krijgsman, W., Wijbrans, J.R., Meulenkamp, J.E., 2006. Late Miocene to Early Pliocene depositional history of the intramontane Florina–Ptolemais–Servia Basin, NW Greece: Interplay between orbital forcing and tectonics. Palaeogeography, Palaeoclimatology, Palaeoecology, 238(1-4), 151-178. DOI: https://doi.org/10.1016/j.palaeo.2006.03.023

Tang, Y., He, W., Wang, R., Ren, H., Jin, Z., Yang, Z., Zhang, Y., 2023. Cyclostratigraphy of Lower Permian alkaline lacustrine deposits in the Mahu Sag, Junggar basin and its stratigraphic implication. Frontiers in Earth Science, 11, 1232418. DOI: https://doi.org/10.3389/feart.2023.1232418

Tian, F., Wang, Y., Liu, J., Tang, W., Jiang, N., 2017. Late Holocene climate change inferred from a lacustrine sedimentary sequence in southern Inner Mongolia, China. Quaternary International, 452, 22-32. DOI: https://doi.org/10.1016/j.quaint.2017.01.029

Tugend, J., Manatschal, G., Kusznir, N.J., 2015. Spatial and temporal evolution of hyperextended rift systems: Implication for the nature, kinematics, and timing of the Iberian-European plate boundary. Geology, 43, 15-18. DOI: https://doi.org/10.1130/G36072.1

Valero, L., Garcés, M., Cabrera, L., Costa, E., Sáez, A., 2014. 20 Myr of eccentricity paced lacustrine cycles in the Cenozoic Ebro Basin. Earth and Planetary Science Letters, 408, 183-193. DOI: https://doi.org/10.1016/j.epsl.2014.10.007

Vickers, M.L., Price, G.D., Jerrett, R.M., Sutton, M., Watkinson, M.P., FitzPatrick, M., 2019. The duration and magnitude of Cretaceous cold events: Evidence from the northern high

latitudes. Geological Society of America Bulletin, 131, 1979-1994. DOI: https://doi.org/10.1130/B35074.1

Vissers, R.L.M., Meijer, P.Th., 2012. Mesozoic rotation of Iberia: Subduction in the Pyrenees? Earth-Science Reviews, 110, 93-110. DOI: https://doi.org/10.1016/j.earscirev.2011.11.001

Walzer, U., Hendel, R., 2023. Natural climate change and glaciations. Earth-Science Reviews, 241, 104435. DOI: https://doi.org/10.1016/j.earscirev.2023.104435

Wang, Y., Deng, T., Flynn, L., Wang, X., Yin, A., Xu, Y., Parker, W., Lochner, E., Zhang, Ch., Biasatti, D., 2012. Late Neogene environmental changes in the central Himalaya related to tectonic uplift and orbital forcing. Journal of Asian Earth Sciences, 44, 62-76. DOI: https://doi.org/10.1016/j.jseaes.2011.05.020

Wang, Y., Huang, C., Sun, B., Quan, C., Wu, J., Lin, Z., 2014. Paleo-CO2 variation trends and the Cretaceous greenhouse climate. Earth-Science Reviews, 129, 136-147. DOI: https://doi.org/10.1016/j.earscirev.2013.11.001

Wang, T., He, S., Zhang, Q., Ding, L., Farnsworth, A., Cai, F., Wang, C., Xie, J., Li, G., Sheng, J., Yue, Y., 2023. Ice Sheet Expansion in the Cretaceous Greenhouse World. Fundamental Research, 1-9. DOI: https://doi.org/10.1016/j.fmre.2023.05.005

Wei, W., Lu, Y., Xing, F., Liu, Z., Pan, L., Algeo, T.J., 2017. Sedimentary facies associations and sequence stratigraphy of source and reservoir rocks of the lacustrine Eocene Niubao Formation (Lunpola Basin, central Tibet). Marine and Petroleum Geology, 86, 1273-1290. DOI: https://doi.org/10.1016/j.marpetgeo.2017.07.032

Wei, Z., Zhong, W., Shang, S., Ye, S., Tang, X., Xiaowen, T., Xue, J., Jibin, X., Jun, O., Smol, J.P., 2018. Lacustrine mineral magnetic record of postglacial environmental changes from Dahu Swamp, southern China. Global and Planetary Change, 170, 62-75. DOI: https://doi.org/10.1016/j.gloplacha.2018.08.010

Wei, X., Yan, D., Luo, P., Jiang, P., Wang, H., Zhou, J., Cong, F., Yang, X., Niu, X., Li, T., Liu, L., Liu, E., 2020. Astronomically forced climate cooling across the Eocene–Oligocene transition in the Pearl river Mouth basin, northern South China Sea. Palaeogeography, Palaeoclimatology, Palaeoecology, 558, 109945. DOI: https://doi.org/10.1016/j.palaeo.2020.109945

Wei, R., Zhang, R., Li, M., Wang, X., Jin, Z., 2023. Obliquity forcing of lake-level changes and organic carbon burial during the Late Paleozoic Ice Age. Global and Planetary Change, 223, 104092. DOI: https://doi.org/10.1016/j.gloplacha.2023.104092.

Woolway, R.I., Kraemer, B.M., Lenters, J.D., Merchant, C.J., O'Reilly, C.M., Sharma, S., 2020. Global lake responses to climate change. Nature Reviews Earth & Environment, 1, 388-403. DOI: https://doi./10.1038/s43017-020-0067-5

Wright, V.P., Marriott, S.B., 1993. The sequence stratigraphy of fluvial depositional systems: the role of floodplain sediment storage. Sedimentary Geology, 86, 203-210. DOI: https://doi.org/10.1016/0037-0738(93)90022-W

Xu, T.-Y., Peng, J., Yu, L.-D., Han, H.-D., Yang, Y.-M., Zeng, Y., Wang, Y.B., 2023. The control of astronomical cycles on lacustrine fine-grained event Sedimentation—A case study of the Chunshang sub-member of the upper Es4 in the Dongying Sag. Petroleum Science, 20(3), 1395-1410. DOI: https://doi.org/10.1016/j.petsci.2022.11.023

Yuste, A., Bauluz, B., Mayayo, M.J., 2015. Genesis and mineral transformations in Lower Cretaceous karst bauxites (NE Spain): climatic influence and superimposed processes. Geological Journal, 50(6), 839-857. DOI: https://doi.org/10.1002/gj.2604

Zavala, C., Liu, H., Li, X., Arcuri, M., Di Meglio, M., Zorzano, A., Otharán, G., Hao, B., Wang, Y., 2022. Lacustrine sequence stratigraphy: New insights from the study of the Yanchang Formation (Middle-Late Triassic), Ordos Basin, China. In: Renchao Yang, A.J., Van Loon, T. (eds.). The Ordos Basin. Sedimentological Research for Hydrocarbons Exploration, 309-335. DOI: https://doi.org/10.1016/B978-0-323-85264-7.00012-6

Zhong, W., Cao, J., Xue, J., Ouyang, J., 2015. A 15,400-year record of climate variation from a subalpine lacustrine sedimentary sequence in the western Nanling Mountains in South China. Quaternary Research, 84(2), 246-254. DOI: https://doi.org/10.1016/j.yqres.2015.06.002

Zhong, Q., Zhang, J.G., Tang, D., Jiang, J.H., Shen, J.J., Cai, M.X., Li, P.X., 2022. Research status of lacustrine mudrock deposition constrained from astronomical forcing. Journal of Palaeogeography, 11(3), 315-331. DOI: https://doi.org/10.1016/j.jop.2022.05.003

Ziegler, A.M., Raymond, A.L., Gierlowski, T.C., Horrell, M.A., Rowley, D.B., Lottes, A.L., 1987. Coal, climate and terrestrial productivity: the present and early Cretaceous compared. London, Geological Society, 32(1, Special Publications), 25-49. DOI: https://doi.org/10.1144/GSL.SP.1987.032.01.04

Manuscript received June 2024;
revision accepted August 2024;
published Online November 2024.